MOLECULAR BIOLOGY

USP7 regulates the ncPRC1 Polycomb axis to stimulate genomic H2AK119ub1 deposition uncoupled from H3K27me3

Ayestha Sijm[1]†, Yaser Atlasi[2]*†, Jan A. van der Knaap[1]†, Joyce Wolf van der Meer[1]†, Gillian E. Chalkley[1], Karel Bezstarosti[1,3], Dick H. W. Dekkers[1,3], Wouter A. S. Doff[1,3], Zeliha Ozgur[4], Wilfred F. J. van IJcken[4], Jeroen A. A. Demmers[1,3]*, C. Peter Verrijzer[1]*‡

Ubiquitin-specific protease 7 (USP7) has been implicated in cancer progression and neurodevelopment. However, its molecular targets remain poorly characterized. We combined quantitative proteomics, transcriptomics, and epigenomics to define the core USP7 network. Our multi-omics analysis reveals USP7 as a control hub that links genome regulation, tumor suppression, and histone H2A ubiquitylation (H2AK119ub1) by noncanonical Polycomb-repressive complexes (ncPRC1s). USP7 strongly stabilizes ncPRC1.6 and, to a lesser extent, ncPRC1.1. Moreover, USP7 represses expression of AUTS2, which suppresses H2A ubiquitylation by ncPRC1.3/5. Collectively, these USP7 activities promote the genomic deposition of H2AK119ub1 by ncPRC1, especially at transcriptionally repressed loci. Notably, USP7-dependent changes in H2AK119ub1 levels are uncoupled from H3K27me3. Even complete loss of the PRC1 catalytic core and H2AK119ub1 has only a limited effect on H3K27me3. Besides defining the USP7 regulome, our results reveal that H2AK119ub1 dosage is largely disconnected from H3K27me3.

INTRODUCTION

Ubiquitin-specific protease 7 (USP7) is a deubiquitylating enzyme that is involved in the regulation of multiple key cellular processes, including tumor suppression, transcription, epigenetics, the DNA damage response, and DNA replication (*1*, *2*). Because of its pivotal function, USP7 is frequently targeted by viral proteins to subvert host cell control, as reflected by its original name: herpesvirus-associated USP (*3*). USP7 is essential for normal development and viability of organisms ranging from *Drosophila* to mammals (*4*, *5*). In humans, USP7 haploinsufficiency causes the neurodevelopmental disorder Hao-Fountain syndrome (OMIM 616863) (*6*, *7*). USP7 also plays a central role in the MDM2-p53 tumor suppressor pathway, where depending on cellular conditions, it acts as either a negative or a positive regulator of p53 (*2*, *8*, *9*). The involvement of USP7 in the MDM2-p53 pathway prompted a major effort to develop selective inhibitors for cancer therapy (*10*). In addition, USP7 has been reported to target an ever-expanding plethora of proteins mainly involved in the maintenance and expression of the genome (*1*, *2*, *11*, *12*). However, USP7's role in epigenetic regulation and specifically in modulating gene repression by the Polycomb system has remained enigmatic. *Drosophila* USP7 was first identified genetically as an enhancer of Polycomb repression (*4*). Subsequent studies in mammalian cells reported a multitude of connections between USP7 and Polycomb (*13*–*18*). Nevertheless, the key molecular mechanism of USP7-mediated regulation of the Polycomb system remains unclear.

Polycomb group (PcG) proteins mediate gene repression as part of two classes of complexes, named Polycomb-repressive complex 1 (PRC1) and PRC2 (*19*–*21*). The key activity of PRC2 is mono-, di-, and trimethylation of histone H3 on lysine 27 (H3K27me3) by EZH1 or EZH2, which is crucial for Polycomb repression (*22*, *23*). The hallmark enzymatic activity of PRC1 is monoubiquitylation of histone H2A at K119 (H2AK119ub1) (*24*–*26*). All PRC1s are assembled around a RING-RING heterodimer, which, in mammals, comprise either RING1A (aka RING1) or RING1B (aka RNF2) paired with one of six PcG finger (PCGF) proteins (*15*, *27*). Although different PRC1s contain additional unique subunits, they are named after the incorporated PCGF1 through PCGF6 (*15*, *19*–*21*, *27*). Association with unique partner proteins leads to the formation of either canonical PRC1 (cPRC1) or noncanonical PRC1 (ncPRC1). The main function of cPRC1s, comprising cPRC1.2 and cPRC1.4, is to mediate chromatin compaction and long-range interactions (*28*, *29*). Pertinently, ncPRC1s rather than cPRC1s are mainly responsible for H2AK119ub1 (*15*, *30*, *31*). There are three types of ncPRC1 complexes: ncPRC1.1, ncPRC1.3/5, and ncPRC1.6. They all share a core of RING1A/B paired with one of PCGF1/3/5/6 that associates with RYBP or its paralog YAF2 and three different sets of partner proteins. Although ncPRC1.1, ncPRC1.3/5, and ncPRC1.6 are differentially recruited to chromatin and have unique properties, they all contribute to H2AK119ub1 modification of chromatin (*26*, *32*–*35*). Generalized hierarchical recruitment models that state that H3K27me3 is necessary for H2AK119ub1 or, more recently, that H2AK119ub1 is required for H3K27me3 permeate the Polycomb field (*32*, *35*, *36*). However, there is accumulating evidence that, rather than a single unified mechanism, different PRCs are recruited through different mechanisms (*19*–*21*). Notably, the degree and order of coupling between H2AK119ub1 and H3K27me3 remain debated (*32*, *35*, *36*, *37*–*40*).

Whereas the role of USP7 in the p53 pathway is well established, a full picture of the USP7 regulatory network is lacking. For example, USP7 has been connected to PRC2 (*16*, *17*), cPRC1 (*13*), SCML2A (*14*), and ncPRC1.1 (*15*, *18*), but the relevant molecular mechanism

[1]Department of Biochemistry, Erasmus University Medical Center, Rotterdam, Netherlands. [2]Patrick G Johnston Centre for Cancer Research, Queen's University Belfast, Belfast, UK. [3]Proteomics Center, Erasmus University Medical Center, Rotterdam, Netherlands. [4]Center for Biomics, Erasmus University Medical Center, Rotterdam, Netherlands.
*Corresponding author. Email: j.demmers@erasmusmc.nl (J.A.A.D.); y.atlasi@qub.ac.uk (Y.A.); c.verrijzer@erasmusmc.nl (C.P.V.)
†These authors contributed equally to this work and should be considered joint first authors.
‡Lead contact.

through which USP7 regulates Polycomb functions remains unclear. To address these questions, we took an unbiased multi-omics approach to define the core USP7 network. Here, we report that USP7 modulates the ncPRC1 axis at the posttranslational level, through stabilization of ncPRC1.6 and ncPRC1.1, and at the transcriptional level, through silencing of ncPRC1.3/5-repressive subunit AUTS2. Consequently, USP7 elevates the global level of H2AK119ub1, especially at loci that undergo transcriptional repression. Our findings reveal that changes in H2AK119ub1 are generally uncoupled from H3K27me3 and thus argue against a hierarchical relationship between these two repressive histone marks.

RESULTS

Mapping the USP7 interaction network shows association with ncPRC1.6

To gain insight into the USP7 network, we performed a series of affinity purifications followed by mass spectrometry (AP-MS). We immunopurified Flag-tagged USP7 (Flag-USP7) from whole-cell extracts (WCEs) prepared from transfected human embryonic kidney (HEK) 293T cells. As a negative control, we used anti-Flag beads for immunoprecipitations (IPs) from WCE from HEK293T cells transfected with an empty vector. All IPs were performed in three biological replicate experiments, and associated proteins were digested on beads and identified by nanoflow liquid chromatography combined with mass spectrometry (nLC-MS/MS). To identify significant interacting proteins, we determined the permutation-based false discovery rate (FDR)–corrected *t* test of protein enrichment in the Flag-USP7 IP versus the control IP (Fig. 1A and data S1). This analysis revealed a set of novel and known USP7-interacting proteins, which are mostly involved in ubiquitin- and chromatin-associated processes. We note the presence of multiple PRC1 subunits, indicated by purple dots (Fig. 1A). As reported earlier (*15*, *18*, *27*), USP7 associated with ncPRC1.1 and all subunits of this complex were readily identified. Likewise, our results confirmed that USP7 binds SCML2 (*14*). However, we did not observe interactions of USP7 with cPRC1 or PRC2. Unexpectedly, we detected USP7 binding to all signature ncPRC1.6 subunits, including PCGF6, MGA, and L3MBTL2. We were intrigued by this novel association, which raised the possibility that USP7 targets ncPRC1.6.

To further define the position of USP7 within the PRC1 network, we determined the interactomes of PCGF1 to PCGF6, RING1A/B, BCOR, MGA, and SCML2 by AP-MS. To complement this analysis, we included USP7-interacting proteins guanosine monophosphate synthase, USP11, DAXX, MAGED2, MCMBP, and TRIM27 (data S1). The results of these 18 (triplicate) AP-MS experiments confirmed the selective association of USP7 with ncPRC1.1, SCML2 and ncPRC1.6, while we did not observe binding to cPRC1 or PRC2 subunits. AP-MS of USP7, PCGF6, and MGA revealed reciprocal binding of these proteins (Fig. 1, A to C). We note large differences in the relative scores of ncPRC1.6 subunits between the PCGF6 and MGA AP-MS experiments. Likewise, the association of BCOR with USP7 is substantially more prominent than with other PRC1.1 subunits (Fig. 1D and fig. S1A). These results suggest that ncPRC1.1 and ncPRC1.6 might represent dynamic protein associations rather than static stoichiometric complexes. AP-MS of TRIM27 confirmed binding to USP7 and a few shared partners but no substantive binding to PRC1.1 or PRC1.6 (fig. S1B). In summary, our AP-MS analyses link USP7 to multiple novel high-confidence partners involved in chromatin-associated processes and ubiquitin regulation. These results and a selection of additional interactions of interest are summarized in Fig. 1E. In the present study, we focus on the role of USP7 in Polycomb regulation.

ncPRC1.6 is the prime Polycomb substrate of USP7

Protein (mono)ubiquitylation can serve a signaling function without affecting protein stability, whereas formation of a polyubiquitin chain via its K48 residue marks cellular proteins for degradation by the 26*S* proteasome. As USP7 can remove both monoubiquitin and K48 polyubiquitin chains, we first examined its role in control of ncPRC1.1 and ncPRC1.6 levels. We compared the relative abundance of key Polycomb proteins and a selection of USP7-associated factors in wild-type (WT) and USP7-KO DLD1 cells. DLD1 colorectal adenocarcinoma cells lack functional p53 due to a S241F mutation. This allowed us to study the role of USP7 without secondary effects due to activation of the p53 pathway, such as apoptosis or cell cycle arrest. To facilitate a comparison of relative protein levels, we used a twofold loading ratio in the immunoblotting analysis. First, we observed markedly reduced levels of ncPRC1.6 subunits PCGF6, MGA, and L3MBTL2 in the absence of USP7 (Fig. 2A). Second, the levels of the ncPRC1.1 subunits BCOR and KDM2B were reduced in cells lacking USP7. Third, our results confirmed that USP7 selectively stabilizes SCML2A but not SCML2B that has a chromatin-independent function in cell cycle regulation (*14*). Last, the levels of Polycomb proteins that were not bound by USP7, such as PCGF4, CBX7, and EZH2, were unaffected by the loss of USP7. We also examined a selection of additional USP7-interacting proteins and found that the levels of TRIM27, TRIP12, USP11, and DHX40 were reduced in USP7 knockout cells, whereas DAXX levels remained stable (Fig. 2B and fig. S2A). In conclusion, our results thus far show that USP7 binds and stabilizes key subunits of ncPRC1.6 and ncPRC1.1.

For a more comprehensive and quantitative approach, we next used parallel reaction monitoring on an Orbitrap mass spectrometer (PRM-MS) to determine the effect of USP7 on the abundance of potential targets. Because of our focus on the relationship between USP7 and the Polycomb system, we surveyed all major PRC1 and PRC2 subunits. For reference, we included a selection of additional proteins associated with USP7. The resulting PRM analysis of 68 different proteins confirmed a profound and selective reduction of key ncPRC1.6 subunits in cells lacking USP7 (Fig. 2, C and D, fig. S2, and data S2). Pertinently, PCGF6, but none of the other PCGFs, was strongly down-regulated. In addition, levels of MGA and L3MBTL2 were reduced substantially. Whereas PCGF6 is essential for H2A ubiquitylation by ncPRC1.6, MGA and L3MBTL2 are crucial for its recruitment to specific genomic loci (*41*–*43*). Thus, USP7 promotes both the targeting and catalytic activity of ncPRC1.6. Loss of USP7 affected KDM2B and BCOR/L1 levels, but not that of other ncPRC1.1 subunits. Notably, the demethylase KDM2B removes the active H3K36me3 mark and recruits ncPRC1.1 to nonmethylated CpG islands (*44*–*46*). PRM-MS also revealed that the levels of TRIM27, TRIP12, and USP11 were dependent on USP7. However, there were no substantial changes in the levels of other high-confidence USP interactors included in our analysis. In contrast to ncPRC1.6 and ncPRC1.1, levels of cPRC1 and PRC2 subunits were largely unaffected by the absence of USP7. However, the ncPRC1.3/5 subunit AUTS2, but not its paralogs FBRS and FBRSL1, was strongly up-regulated in USP7 null cells (Fig. 2E). AUTS2 recruits the kinase

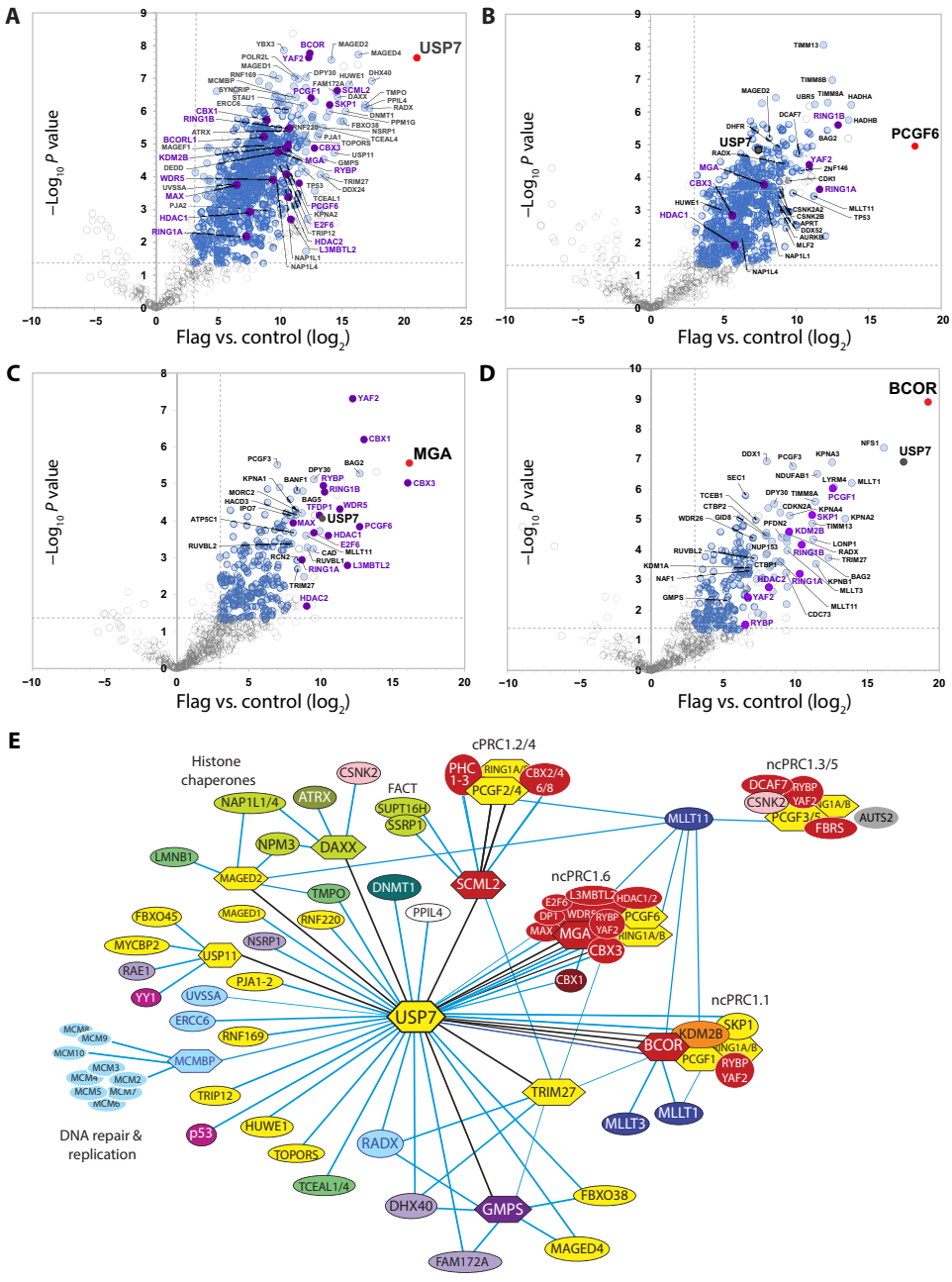

Fig. 1. Systematic mapping of the USP7 network. (**A**) Proteins associated with Flag-USP7 purified from HEK293T cells. Volcano plot in which the permutation-based FDR-corrected *t* test difference of the $\log_2$ iBAQ values of Flag-USP7 IPs versus control Flag-IPs from cells lacking Flag-USP7 is plotted against the negative $\log_{10}$ *P* value of the test. The analysis is based on three independent biological replicate experiments. Note that the Flag-USP7 bait protein was overexpressed (~20-fold as based on LFQ quantitation). Bait is indicated in red, and Polycomb proteins are in purple. Gray circles depict common contaminants such as ribosomal proteins or insignificant hits. For original data, see data S1. (**B** to **D**) AP-MS analysis of Flag-PCGF6, Flag-MGA, and Flag-BCOR. (**E**) USP7-centered interaction network. A schematic summary of the results of a series of 18 triplicate AP-MS experiments using Flag-tagged bait proteins, which are depicted as hexagons. Black lines indicate associations detected in both IP directions (i.e., between hexagons). Blue lines represent interactions detected in one direction, either because it only had a high score in IPs in one direction or because the partner protein was not used as a bait in a reverse-IP. PRC1 subunits are depicted as part of established complexes. We indicated a selection of high-confidence interactions. Yellow, ubiquitin regulation; red, Polycomb; green, histone chaperones and chromatin regulation; light blue, DNA repair and replication; pink, kinase; purple, RNA regulation. AUTS2 is depicted in gray because of its low iBAQ score. See also fig. S1. For the complete dataset, see data S1.

CSNK2A/B to ncPRC1.3/5, which, in turn, inhibits H2AK119 ubiquitylation through phosphorylation of RING1A/B (*47*). In addition, AUTS2 binds the histone acetyltransferase P300/CBP, a transcriptional coactivator. Combined, these activities convert AUTS2-PRC1.3/5 into a transcriptional activator (*47*). Thus, USP7 appears to repress expression of the AUTS2 inhibitor of H2AK119 ubiquitylation by ncPRC1.3/5. Because ncPRC1s mediate H2AK119ub1, we examined the effect of USP7 loss on this histone mark. Immunoblot analyses

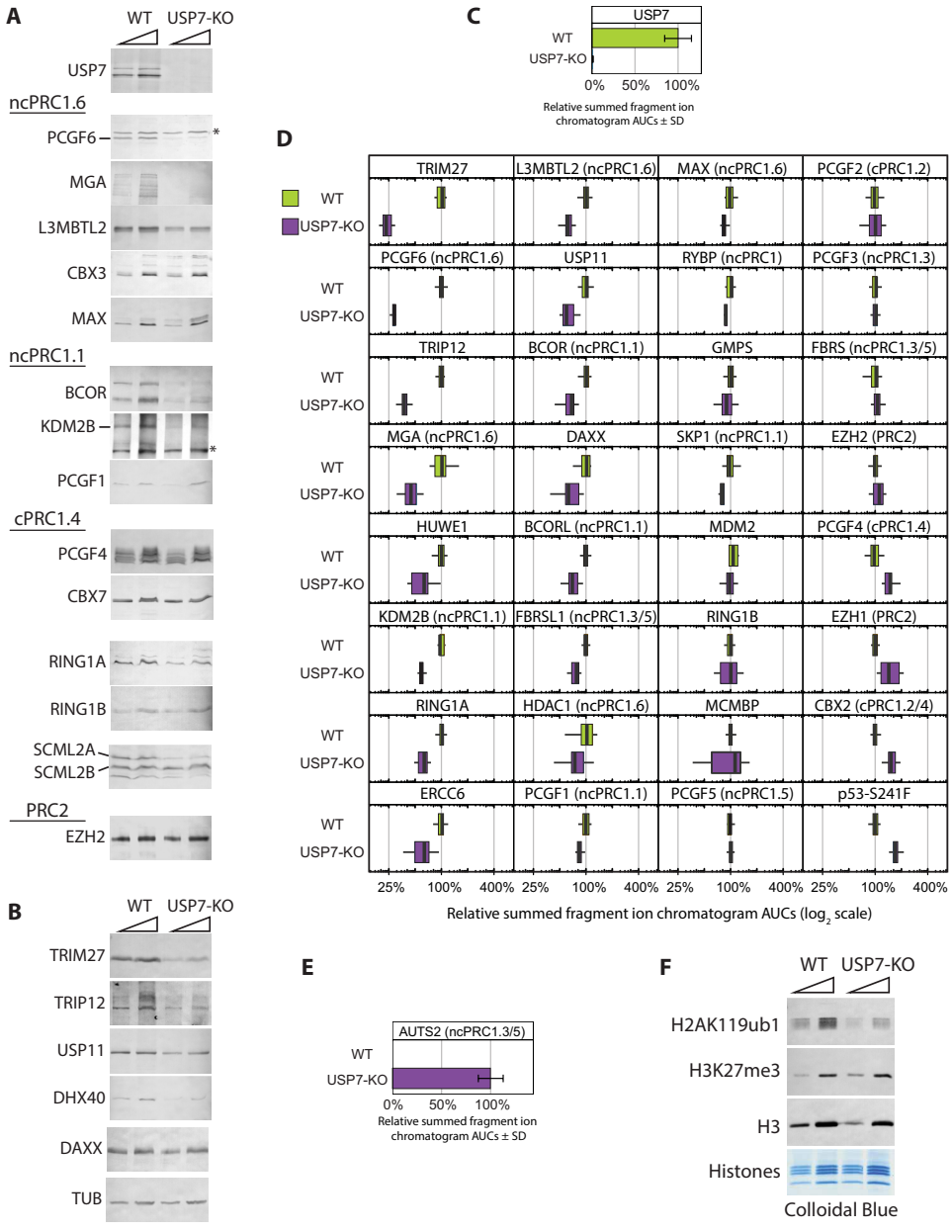

Fig. 2. Effect of USP7-KO on target protein abundance and the Polycomb system. (**A** and **B**) Immunoblot analysis of WCEs from WT or USP7-KO DLD1 cell. Triangles indicate a twofold loading ration for each sample. The asterisk indicates background bands. Tubulin (TUB) serves as a loading control. (**C** to **E**) PRM analysis of protein abundance in WT (green) and USP7-KO DLD1 cells (purple). Relative summed fragment ion chromatogram areas under the curve (AUCs) were determined for ≥2 peptides per protein averaged over three biological replicates, each processed in two technical replicate analyses. The resulting six values were normalized for each peptide detected in WT cells and then summed to derive a value for each protein. For USP7 (B) and AUTS2 (D), we set the value in WT or USP7-KO cells at 100% because no or extremely low signals were detected in USP7-KO cells or WT cells, respectively. To plot changes in protein abundance in (C), protein values from USP7-KO cells were expressed relative to those from WT cells. The median for WT cells was set to 100%. Boxplot, interquartile range (IQR) from Q1 to Q3 (equal to 25 to 75th percentiles); bar, median; whiskers, minimum at Q1 − 1.5*IQR and maximum at Q3 + 1.5*IQR. For details, see Materials and Methods. For the complete dataset, see fig. S2 and data S2. (**F**) Immunoblot analysis of acid-extracted histones isolated from either WT or USP7-KO cells, probed with antibodies directed against H2AK119ub1, H3K27me3, or unmodified H3. For each sample, a twofold loading ratio was used. Bulk histones were analyzed by colloidal blue staining.

revealed an about twofold reduction in the level of H2AK119ub1 in USP7-deficient cells compared to WT cells (Fig. 2F). In contrast, there was no corresponding drop in H3K27me3 levels. Loss of USP7 in another cell line, HCT116, also caused reduced levels of PCGF6 and H2AK119ub1, without affecting H3K27me3 (fig. S2C). We conclude that, at least on the level of bulk chromatin, there is no obligatory coupling between these two Polycomb marks.

To generate a switchable system to study USP7 function, we introduced green fluorescent protein (GFP)–tagged USP7 under control of a doxycycline (Dox)–inducible promoter into the DLD1 USP7-KO

cell line to generate DLD1-KO-Dox-USP7 (Fig. 3, A and B). Next, we examined the effects of USP7 reexpression on its target proteins by PRM-MS. We determined protein levels in extracts from cells before USP7 induction and after 1, 3, or 9 days of USP7 expression by Dox treatment (Fig. 3C, fig. S3, and table S3). PCGF6 was the most up-regulated protein after USP7 induction. In addition, we observed strongly increased levels of MDM2, TRIM27, TRIP12, and MGA. Moreover, USP11, p53-S241F, ERCC6, L3MBTL2, and KDM2B were stabilized by USP7. However, USP7 reexpression had only a minor effect on the abundance of RING1A/B and BCOR/L1. In contrast to the other ncPRC1.3/5 subunits, AUTS2 was down-regulated upon induction of USP7 (Fig. 3D). Last, our analysis again did not reveal substantial change in the levels of cPRC1 or PRC2 subunits.

To test whether protein stabilization was dependent on USP7's deubiquitylation activity, we cotransfected vectors expressing selective substrates with vectors expressing either no protein (–), WT USP7, or catalytically inactive USP7-C223S (*4*, *9*) in U2OS USP7-KO cells (Fig. 4A). USP7, but not USP7-C223S, robustly stabilized PCGF6, L3MBTL2, and MDM2. Likewise, stabilization of TRIM27, TRIP12, KDM2B, and BCOR was also dependent on USP7 deubiquitylation activity. As expected, the protein level of the noninteracting PCGF2 was not affected by USP7. USP7's catalytic activity was crucial for RING1A and RING1B stabilization when they partnered with PCGF6 (Fig. 4B). Albeit less prominently, USP7 activity also increased levels of RING1A/B-PCGF1 dimers (Fig. 4C). In contrast, RING1A/B-PCGF4 abundance was independent of USP7 (Fig. 4D). When expressed alone, RING1A/B levels were independent of USP7 (Fig. 4E).

In conclusion, our results establish ncPRC1.6 as the predominant USP7 target. USP7 is required for the stability of its RING1A/B-PCGF6 catalytic core and that of the recruiting subunits MGA and L3MBTL2. USP7 also modestly promotes the levels of key ncPRC1.1 subunits. Last, either directly or indirectly, USP7 represses AUTS2, an inhibitor of the H2AK119ub1 activity of ncPRC1.3/5. These combined effects of USP7 result in increased levels of H2AK119ub1.

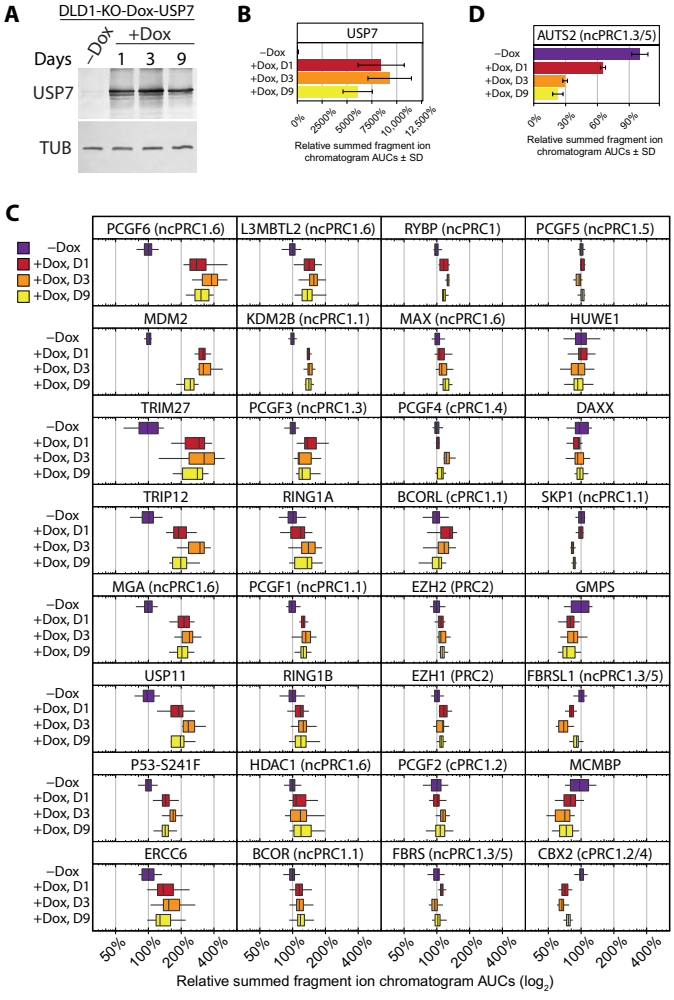

Fig. 3. Effect of USP7 re-expression on target protein levels. (**A**) Immunoblot analysis of Dox-inducible GFP-USP7 in DLD1-KO-Dox-USP7 cells before USP7 induction and 1, 3, or 9 days after addition of Dox. Tubulin (TUB) serves as a loading control. (**B** to **D**) PRM analysis of relative protein abundance in DLD1-KO-Dox-USP7 cells before USP7 induction (–Dox, purple) and 1 (red), 3 (orange), or 9 (yellow) days after addition of Dox. Analysis as described for Fig. 2. The median protein abundance in –Dox cells was set to 100%. For the complete dataset, see fig. S3 and data S3.

USP7 modulates developmental and oncogenic transcription programs

To determine the impact of USP7 on gene transcription, we compared the RNA sequencing (RNA-seq) profiles of DLD1-KO-Dox-USP7 cells before and after expression of USP7 for 1, 3, or 9 days. As a reference, we used WT DLD1 cells. mRNA was isolated from three independent biological replicates. Principal components analysis of the sequenced mRNA showed that rescuing USP7 alters the gene expression in USP7-KO cells, gradually shifting the expression profiles toward the profile of WT cells (Fig. 5A). These slow and continuous changes in mRNA expression indicate largely indirect effects of USP7 on gene transcription. Reflecting its diverse protein targets, comparable numbers of genes were up- or down-regulated following induction of USP7. Using differential gene expression analysis, we identified 235 genes that were up-regulated and 196 genes that were down-regulated more than twofold by USP7 (FDR < 0.05). More than half of the differentially expressed genes in USP7-KO versus WT cells were rescued by reexpression of USP7 (Fig. 5B and fig. S4A). Given that DLD1 cells lack functional p53, these results show that USP7 has a substantial impact on transcription that is independent of the p53 pathway.

Gene ontology (GO) term enrichment analysis showed that genes up-regulated by USP7 are largely associated with metabolic processes and extracellular matrix interactions, whereas genes repressed by USP7 are mainly involved in morphogenesis and differentiation (fig. S4B). mRNA expression analysis revealed that USP7 controls *AUTS2* expression at the level of transcription (Fig. 5C; see also Figs. 2, D and E, and 3, C and D). In contrast, expression of the *AUTS2* paralogs *FBRS* and *FBRSL1* remained unchanged. Note that mRNA levels of targets that were stabilized at the protein level, such as PCGF6, MGA, and L3MBTL2, were unaffected by USP7 expression (compare Figs. 3C and 5C). USP7 regulates the *H19-IGF2* locus, which plays multiple roles in growth control and cancer (*48*). USP7 strongly attenuates expression of the *H19* long noncoding RNA, whereas *IGF2*, which is silenced by expression of *H19*, is induced by USP7. Other genes repressed by USP7 include the neurexin *CTNAP2*; the apoptotic regulator *BCL2*; signaling factors *WNT11* and *WNT10B*; and developmental transcription factors *GLI2*, *PAX6*, *HOXD8*, *OTX1*, and *HOPX*. These results implicate USP7 in

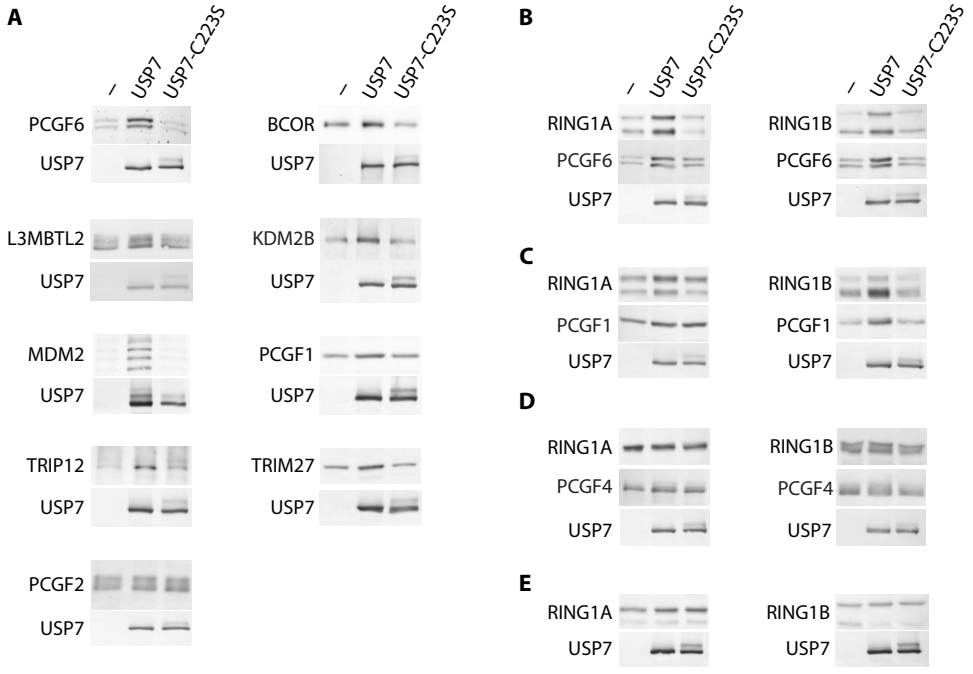

Fig. 4. USP7 activity stabilizes key subunits of ncPRC1.6 and ncPRC1.1. (**A**) Immunoblot analysis of USP7-KO cells transfected with an empty vector (–) or a vector expressing the indicated USP7 target proteins, in combination with either WT USP7 or the catalytically inactive mutant USP7-C223S. (**B** to **E**) Similar analysis as described above for RING1A or RING1B coexpressed with either PCGF6, PCGF1, PCGF4, or without a PCGF partner.

the transcriptional regulation of key developmental and oncogenic pathways.

USP7 stimulates genomic H2AK119ub1 deposition uncoupled from H3K27me3

Our results established that USP7 modulates the Polycomb system at the posttranslational level, through stabilization of ncPRC1.6 and ncPRC1.1, and at the transcriptional level, through silencing of *AUTS2*. Consequently, reexpression of USP7 in DLD1-KO-Dox-USP7 cells resulted in increased levels of H2AK119ub1 (Fig. 6A). In contrast, the levels of H3K27me3 remained unaffected. To determine the effects of USP7 on H2AK119ub1 and H3K27me3 at the genomic level, we used chromatin IP with reference exogenous genome (ChIP-Rx) (*49*), allowing a direct and quantitative comparison between histone modifications in cells lacking or expressing USP7. We compared the genomic distribution of H2AK119ub1 and H3K27me3 on chromatin in DLD1-KO-Dox-USP7 cells before or following induction of USP7 for 3 days. As a normalization reference, we spiked in *Drosophila* chromatin. We identified 28,722 H2AK119ub1 and 30,751 H3K27me3 peaks using SICER, a computational algorithm specifically developed for broad-peak calling (*50*). Quantification of read counts in all identified peaks confirmed that USP7 reexpression increased global deposition of H2AK119ub1. However, there was no correlation between changes in H2AK119ub1 and changes in H3K27me3 across all peaks identified (Fig. 6B). Further analysis of these two histone modifications identified three classes of genomic loci: cluster 1 sites (n = 13,802) that are marked by both H2AK119ub1 and H3K27me3, cluster 2 sites (n = 14,875) that are marked by H2AK119ub1 but not by H3K27me3, and cluster 3 sites (n = 16,773) that are marked by H3K27me3 but largely devoid of H2AK119ub1 (Fig. 6C). Genomic regions marked by H2AK119ub1 and H3K27 (cluster 1) or only H2AK119ub1 (cluster 2) were mainly enriched at promoters and CpG islands (fig. S5A). Regions marked by H3K27me3, but not by H2AK119ub1 (cluster 3), were enriched for intergenic regions and long terminal repeats. Heatmaps and plotting of averaged signals showed that USP7 strongly induces H2AK119ub1 deposition across the genome but does not cause an appreciable change in H3K27me3 (Fig. 6, C and D). Note that the presence (cluster 1) or absence (cluster 2) of H3K27me3 had no effect on the stimulation of H2AK119ub1 by USP7. Last, analysis of loci with the highest changes in H2AK119Ub in response to USP7 expression showed no difference in H3K27me3 (fig. S5B).

Next, we explored the relationship between H2AK119ub1- and USP7-induced changes in gene expression (Fig. 6, E and F). Repression by USP7 was accompanied by a strong induction of H2AK119ub1 at the promoter regions, whereas the level of H3K27me3 remained low and unaffected (Fig. 6F, top). In contrast, genes that were activated by USP7 displayed little change in their low levels of H2AK119ub1 and H3K27me3 (Fig. 6F, bottom). Genome browser views of genes repressed by USP7 illustrate increased H2AK119ub1 in the absence of notable changes in H3K27me3 (Fig. 6G). These results indicate that USP7 mediates gene repression by stimulating H2AK119ub1 deposition by ncPRC1s. USP7-induced gene activation is likely to be indirect, involving other protein targets.

As an additional test of the relationship between H2AK119ub1 and H3K27me3, we generated DLD1 cells that lack both RING1A and RING1B (RING1A/B-KO), thus disabling the complete PRC1 axis of the Polycomb system. Immunoblotting showed that RING1A/B-KO cells lack H2AK119ub1, whereas the level of H3K27me3 remained comparable to that in WT cells (Fig. 7A). Likewise, targeted degradation of RING1B in DLD1 cells lacking endogenous RING1A/B resulted in reduced levels of H2AK119ub1 without affecting

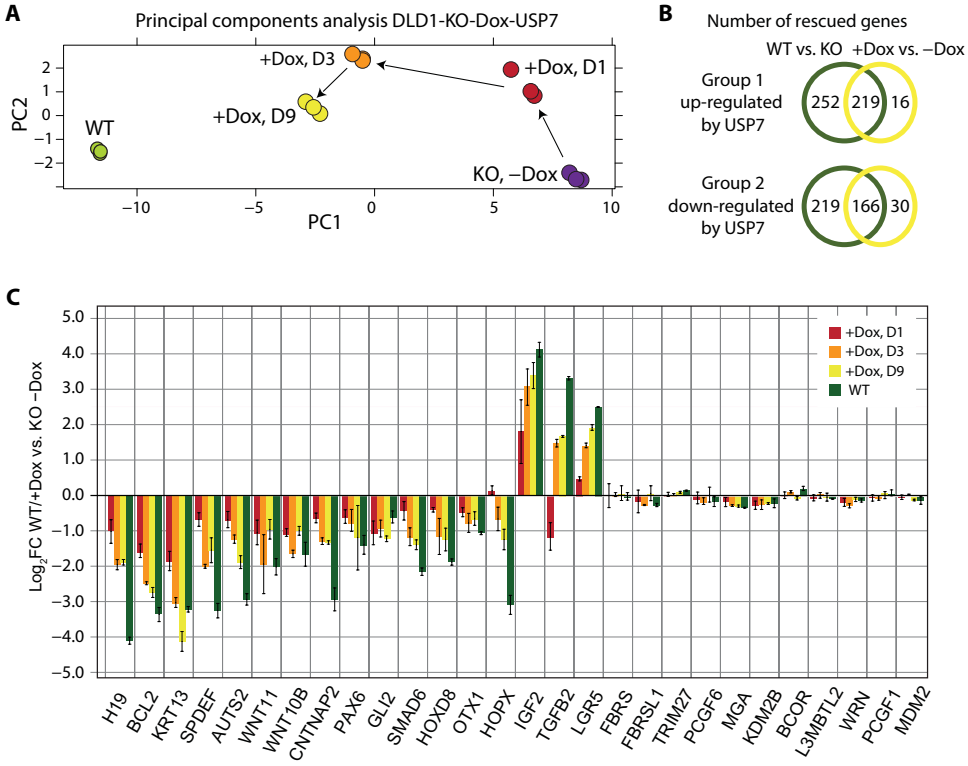

Fig. 5. Impact of USP7 on gene transcription. (**A**) Principal components analysis of RNA-seq data from DLD1-KO-Dox-USP7 cells before USP7 induction (−Dox, purple) and 1 (red), 3 (orange), or 9 (yellow) days after addition of Dox. DLD1 WT cells (green) were used as a reference. For each condition, three independent biological replicates were used. (**B**) Venn diagram showing the rescue of a large portion of differentially expressed genes (>2-fold, FDR < 0.05) in WT versus USP7-KO cells by reexpression of USP7 (+Dox). (**C**) Selection of transcriptionally regulated genes in response to USP7 reexpression. Changes in expression are presented as fold change relative to DLD1-KO-Dox-USP7 cells grown −Dox. We included examples of genes regulated at the protein level (e.g., *PCGF6*, *MGA*, and *TRIM27*) and the paralogs of *AUTS2*: *FBRS* and *FBRSL1*. Values were based on RNA-seq data. Means and SDs were derived from three biological replicates. For RNA-seq data, see data S4.

H3K27me3 (fig. S6A). Next, we introduced either WT RING1A or a catalytically inactive RING1A-I50S (*41*) or RING1A-C72A under control of a Dox-inducible promoter into the DLD1 RING1A/B-KO cell line to generate DLD1-DKO-Dox-RING1A. In the absence of Dox, we could not detect H2AK119ub1. Induction of WT RING1A, but not RING1A-I50S or RING1A-C72A, partially restored H2AK119ub1 (Fig. 7B). However, the absence or presence of H2AK119ub1 did not affect the level of H3K27me3. Likewise, the loss of both RING1A and RING1B in HAP1 cells caused a complete loss of H2AK119ub1 without affecting the bulk level of H3K27me3, which remained comparable to that in WT cells (Fig. 7C). Direct comparison of all 30,751 or 34,703 H3K27me3 peaks identified by ChIP-Rx-seq in DLD1 or HAP1 cells, respectively, did not show substantial differences upon loss of H2AK119ub1 (Fig. 7D and fig. S6B). Scatter plot comparisons of H3K27me3 peaks in cells that either express or lack RING1A/B established that there are no significant differences for most loci (Fig. 7E). Approximately 7% of H3K27me3 peaks identified in either DLD1 or HAP1 cells showed more than twofold reduction in signal in the absence of RING1A/B and H2AK119ub1 (Fig. 7F). A significant portion of these loci are associated with genes involved in (neuro)development (fig. S6C). Notably, in both DLD1 and HAP1 cells, RING1A/B-dependent H3K27me3 peaks are significantly enriched for *HOX* genes (hypergeometric enrichment test P value = 3.588×10^{-5} for 1950 loci in DLD1 cells and P value = 4.84×10^{-11} for 2340 loci in HAP1 cells). Such an enrichment was not observed when an equal number of randomly selected H3K27me3 loci were tested ($P = 0.493$ and $P = 0.3$ for DLD1 and HAP1 cells, respectively). These results are illustrated by genome browser views of representative loci (fig. S6D). We conclude that the coupling between H2AK119ub1 and H3K27me3 is context dependent rather than universal.

Our PRM-MS and RNA-seq analysis indicated that, directly or indirectly, USP7 controls *AUTS2* expression at the level of transcription (Figs. 3D and 5C). We wondered whether repression of *AUTS2* by USP7 might be dependent on PRC1. Reverse transcription quantitative polymerase chain reaction (RT-qPCR) showed that loss of either USP7 or RING1A/B caused a similar induction of *AUTS2* expression in DLD1 cells (Fig. 7G). In contrast, expression of *FBRS* and *FBRSL1* remained unchanged. Reexpression of RING1A in DLD1-DKO-Dox-RING1A cells partially restored repression of *AUTS2*, whereas expression of RING1AI50S or RING1A-C72A had no effect (Fig. 7H). Last, loss of RING1A/B in HAP1 cells also caused derepression of *AUTS2* transcription (Fig. 7I). Consequently, AUTS2 protein is up-regulated in HAP1 RING1A/B-KO cells, as shown by PRM-MS (fig. S6E). Collectively, these results indicate that USP7 might modulate transcriptional repression of *AUTS2* via the ncPRC1 axis. Indeed, H2AK119ub1 at the *AUTS2* locus is reduced in the absence of USP7 (Fig. 7J). Inspection of CUT&RUN data of L3MBTL2 and MGA (*43*) showed binding at the *AUTS2* locus (Fig. 7J), indicating that PRC1.6 plays a role in the regulation of the *AUTS2* gene.

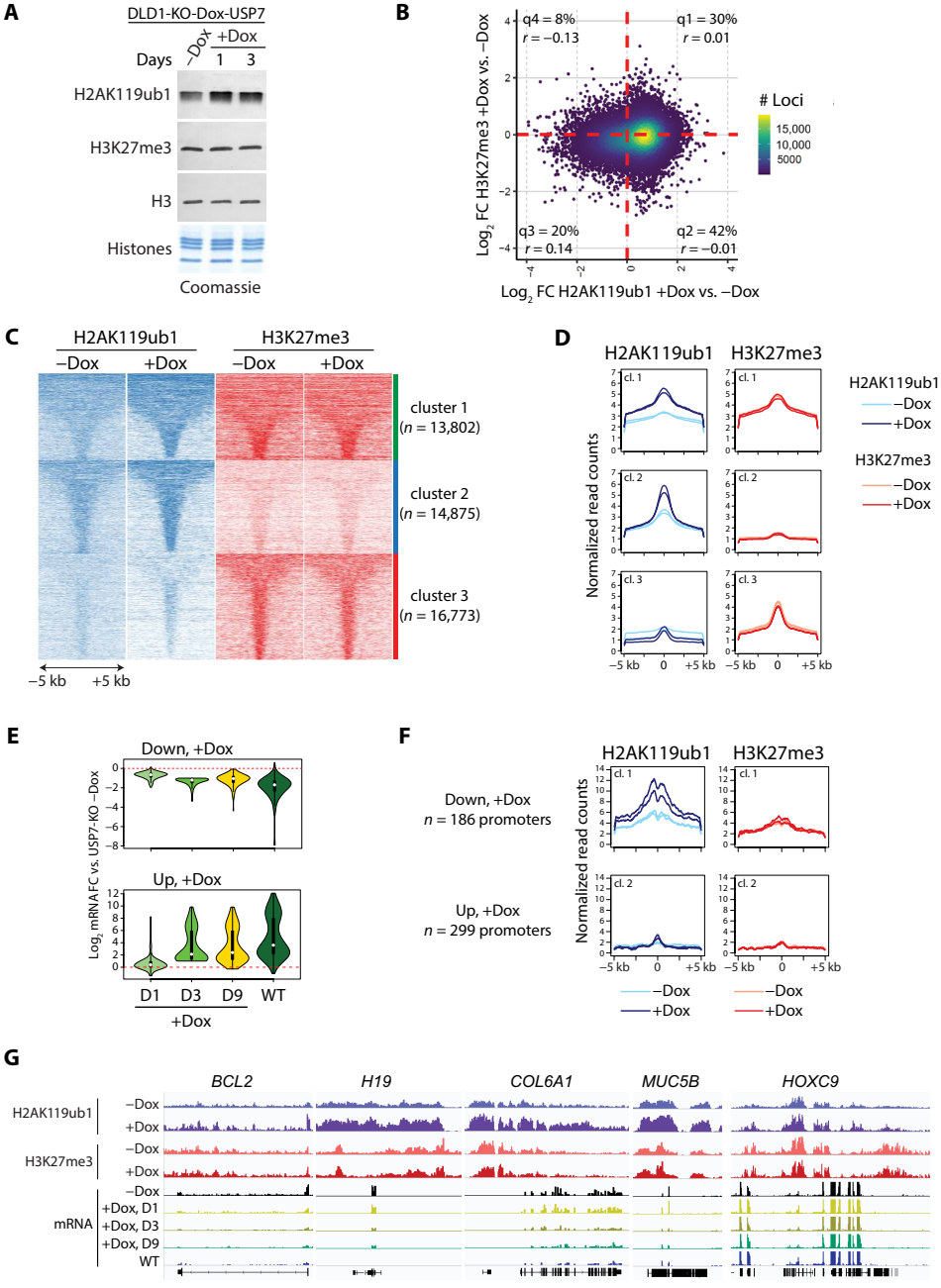

Fig. 6. USP7 promotes H2AK119ub1 deposition uncoupled from H3K27me3. (**A**) Immunoblot analysis of histones isolated from DLD1-KO-Dox-USP7 cells. (**B**) Scatter plot of changes in H3K27me3 (day 3, +Dox versus −Dox) plotted against changes in H2AK119ub1 across all detected ChIP-Rx-seq peaks. Each dot represents the average fold change of two biological replicates per group. (**C**) Heatmap showing the H2AK119ub1 and H3K27me3 signals in DLD1-KO-Dox-USP7 grown without Dox and in the presence of Dox for 3 days. Average ChIP-seq read counts of two biological replicates are visualized in 100-bp bins in 10-kb windows. (**D**) Average plots showing the quantification of H2AK119ub1 and H3K27me3 mean signals across promoters of genes, corresponding to clusters 1 to 3, for two biological replicates per condition. (**E**) Violin plots showing the down- or up-regulation of gene expression following induction of USP7 (selected at day 3) relative to that in uninduced cells (−Dox). The thick line indicates the interquartile range; median is indicated by a white dot. Plots are based on three biological replicates. (**F**) Average plotted quantification of H2AK119ub1 and H3K27me3 mean signals across promoters of genes that are either repressed (top) or activated (bottom) by USP7, for two biological replicates. (**G**) Genome browser view of H2AK119ub1 and H3K27me3 at representative genomic loci and corresponding mRNA levels detected by RNA-seq. Each track represents the merged reads derived from two biological replicates. For ChIP-Rx-seq data, see table S5.

In summary, USP7 modulates the ncPRC1 axis at both the post-translational level (by stabilization of ncPRC1.6 and ncPRC1.1) and at the transcription level, through PRC1-dependent transcriptional repression of the ncPRC1.3/5 repressive subunit AUTS2 (Fig. 8). USP7-regulated changes in H2AK119ub1 do not generally affect the level and distribution of H3K27me3. Even a complete loss of RING1A/B and H2AK119ub1 has only a restricted effect on H3K27me3. These data show that there is no general coupling between H2AK119ub1 and H3K27me3.

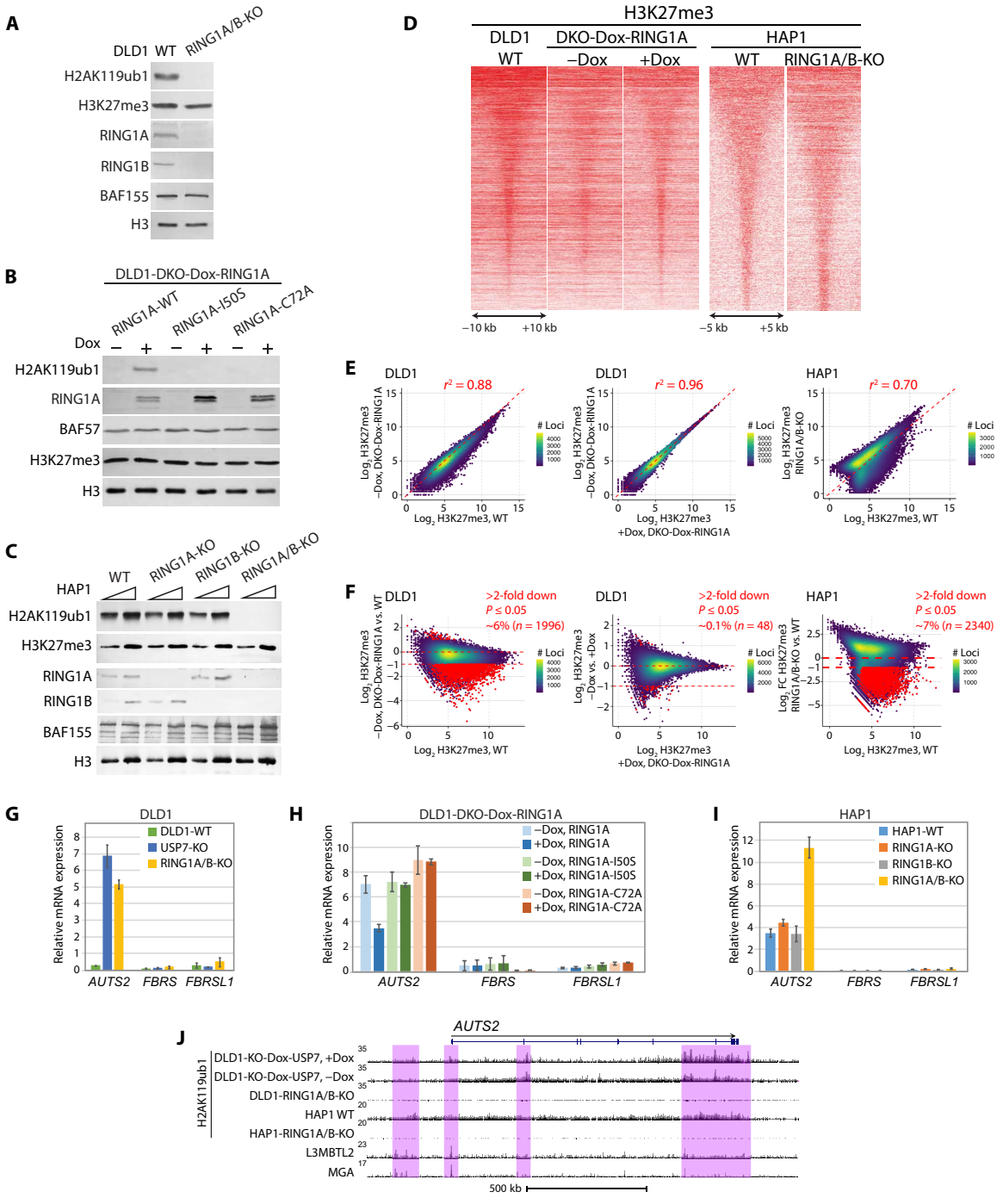

Fig. 7. H2AK119ub1 and H3K27me3 are largely independent. (**A** to **C**) Immunoblot analysis of (A) RING1A/B-KO DLD1 cells; (B) DLD1-DKO-Dox-RING1A, DLD1-DKO-Dox-RING1A-I50S, and DLD1-DKO-Dox-RING1A-C72A (–Dox or +Dox); and (C) WT, RING1A-KO, RING1B-KO, and RING1A/B-KO HAP1 cells. (**D**) Heatmap showing the H3K27me3 signals across 30,751 H3K27me3 peaks identified in WT DLD1 and DLD1-DKO-Dox-RING1A cells (–Dox or +Dox) and across 34,703 H3K27me3 peaks identified in WT and RING1A/B-KO HAP1 cells. See fig. S6B for replicates. (**E**) Scatter plot comparisons of all H3K27me3 peaks detected in DLD1 or HAP1 cells that either express or lack RING1A/B. Each dot represents the average H3K27me3 intensity across two biological replicates per group. Pearson correlation coefficients are indicated. (**F**) Log_2 fold change in H3K27me3 signal in cells lacking RING1A/B versus cells expressing RING1A/B, plotted against the H3K27me3 signal in cells that express RING1A/B. Red dots indicate H3K27me3 peaks that showed a more than twofold reduction in signal in RING1A/B-deficient cells compared to expressing cells with a $P \leq 0.05$. For data, see tables S6 and S7. (**G**) RT-qPCR analysis of mRNA levels of *AUTS2*, *FBRS*, and *FBRSL1* in WT DLD1, USP7-KO, and RING1A/B-KO cells. Means and SEM were derived from three biological replicates. (**H**) Similar analysis for DLD1-DKO-Dox-RING1A, DLD1-DKO-Dox-RING1A-I50S, and DLD1-DKO-Dox-RING1A-C72A (–Dox or +Dox). (**I**) RT-qPCR analysis of WT HAP1, RING1A-KO, RING1B-KO, and RING1A/B-KO cells. (**J**) Genome browser view of H2AK119ub1 at the *AUTS2* locus. The L3MBTL2 and MGA tracks are based on CUT&RUN data from reference (*43*).

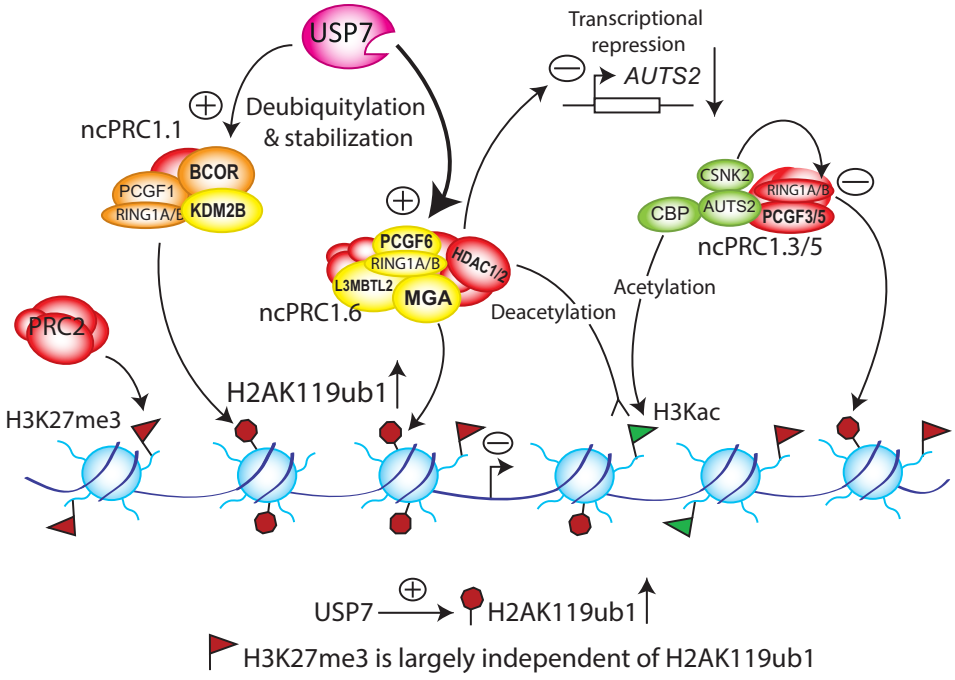

Fig. 8. Model for regulation of the Polycomb system by USP7. USP7 stabilizes ncPRC1.6 and, albeit less prominently, ncPRC1.1. ncPRC1 subunits that depend strongly on USP7 are depicted in yellow. USP7 stabilizes MGA and L3MBTL2, which mediate recruitment of ncPRC1.6 to the genome, and the RING1A/B-PCGF6 catalytic core. Moreover, USP7 activity stabilizes KDM2B, which recruits ncPRC1.1 to CpG islands. The effects of USP7 on BCOR and the PCGF1-RING1A/B catalytic core are modest and somewhat variable in our assays (indicated in orange). In addition, USP7 is responsible for the transcriptional repression of the *AUTS2* gene. AUTS2 protein inhibits the H2A ubiquitylation activity of ncPRC1.3/5 by stimulating its phosphorylation by CSNK2A/B and turns it into a transcriptional activator by linking it to the CBP/p300 histone acetyltransferase. The AUTS2-dependent activating module is shown in green. We speculate that USP7 mainly represses *AUTS2* transcription indirectly, via stabilization of PRC1.6. Collectively, stabilization of ncPRC1.6 and PRC1.1, as well as opposition of AUTS2, leads to increased deposition of H2AK119ub1. However, changes in H2AK119ub1 are largely uncoupled from H3K27me3 by PRC2.

DISCUSSION

Integrating unbiased proteomics, genomic, and functional molecular approaches, we determined the core USP7 regulatory circuitry. Our identification of high-confidence targets established USP7 as a regulatory hub in a multinodal network involved in tumor biology, protein (de)ubiquitylation, and genome regulation. Combined, our multi-omics results provide a resource for future studies on the role of USP7 in (neuro)development and cancer. Here, we followed-up on the regulation of the Polycomb system by USP7. We established that ncPRC1.6 is the prime target of USP7. USP7 stabilizes MGA and L3MBTL2, which direct ncPRC1.6 to the genome (*41*–*43*), and the RING1A/B-PCGF6 catalytic core (Fig. 8). Moreover, USP7 activity stabilizes KDM2B, which recruits ncPRC1.1 to CpG islands (*44*–*46*). Albeit more modestly, USP7 also stabilizes BCOR and the RING1A/B-PCGF1 enzymatic core of PRC1.1. Last, USP7 opposes expression of AUTS2, the subunit that suppresses H2A ubiquitylation by ncPRC1.3/5 (*47*). Collectively, these USP7 activities increase the genomic deposition of H2AK119ub1. Contradicting prevalent paradigms of Polycomb function, our results argue against an obligatory hierarchical relationship between H2AK119ub1 and H3K27me3.

Whereas loss of USP7 leads to reduced H2AK119ub1, we observed no substantial effects on either the bulk level or the genomic distribution of H3K27me3. Unbiased identification of H2AK119ub1 and H3K27me3 distribution in DLD1 cells by ChIP-Rx-seq showed that these histone marks coexist at about a third of their loci (Fig. 6C and fig S5A). Thus, while there is substantial overlap, H2AK119ub1 and H3K27me3 are not globally coincident. Pertinently, there was no correspondence between USP7-dependent changes in H2AK119ub1 and H3K27me3 (Fig. 6). In RING1A/B-KO cells, there is no detectable H2AK119ub1, whereas H3K27me3 levels and genomic distribution are largely similar to that in WT cells (Fig. 7). Only at a minority of loci in RING1A/B-KO cells did we observed a reduction in H3K27me3. Notably, these RING1A/B-dependent H3K27me3 loci are significantly enriched for *HOX* genes, which are canonical Polycomb targets. Thus, the coupling between H2AK119ub1 and H3K27me3 is context dependent rather than universal. Our results dovetail well with observations in different physiological systems that showed largely independent or redundant pathways centered on H2AK119ub1 and H3K27me3 (*37*–*40*, *51*, *52*). Rather than a generalized hierarchical mechanism, cross-talk between PRC1 and PRC2 is subcomplex specific (*19*–*21*). For example, binding of cPRC1 CBX subunits to H3K27me3, or recognition of H2AK119ub1 by PRC2 accessory factors JARID2 or AEBP2, allows for context-dependent communication between PRC1 and PRC2 class complexes during developmental gene regulation (*19*–*21*, *53*).

USP7 haploinsufficiency causes Hao-Fountain syndrome (7, 8; OMIM 616863), but the molecular targets responsible for this neurodevelopmental disorder remain unclear. Previously, a role for USP7 in endosomal protein recycling via stabilization of MAGEL2-TRIM27 was proposed to contribute to Hao-Fountain syndrome (*7*). We note, however, that USP7 is a predominantly nuclear protein and mutations in several of its nuclear targets, including, e.g., BCOR, RING1A, KDM2B, and ERCC6, have been implicated in a variety of neurodevelopmental syndromes (*26*, *54*–*57*). Last, USP7 regulates

the expression of developmental genes, such as *AUTS2*, that play important roles in neurodevelopment and autism spectrum disorders (*26*, *47*). Thus, our proteomic and transcriptomic analyses uncovered USP7 targets that are promising candidates for the molecular pathways underpinning Hao-Fountain syndrome. We propose that epigenetic control by USP7 may be highly relevant for pathogenesis in the Hao-Fountain syndrome.

The connection of USP7 to the Polycomb system suggests that its role in cancer extends beyond regulation of p53. The stabilization of ncPRC1.6 links USP7 to the MYC oncogenic network. Amplification and overexpression of the MYC transcription factor is a major oncogenic driver in many human cancers. MYC broadly stimulates transcription and functions as part of a network of transcription factors that can either enhance or antagonize its activity (*58*). MYC binds to its target DNA sites as a MYC-MAX dimer and stimulates the expression of a multitude of growth-promoting genes. This tumor-driving activity of MYC is opposed by MGA-ncPRC1.6 that attenuates expression of genes activated by MYC-MAX (*43*, *59*). In addition, PCGF6 can suppress Myc-induced lymphomagenesis, which appears to be independent from MGA-PRC1.6 and transcriptional regulation (*60*). Thus, USP7 is involved in the regulation of both the p53 tumor suppression pathway and the MYC oncogenic network. Similar to MGA-ncPRC1.6, BCOR-ncPRC1.1 is a bona fide tumor suppressor complex. Aberrations in BCOR, including gene fusions, tandem duplications, and loss-of-function mutations, act as drivers in sarcomas, neuronal tumors, T cell leukemias, and other hematological tumors (*61*). Moreover, ncPRC1.1 subunit KDM2B also functions as a tumor suppressor in T cell leukemogenesis (*62*). These observations suggest that USP7 might promote tumor suppression through deubiquitylation of selective ncPRC1 subunits. Notably, *USP7* is among the most frequently mutated genes in pediatric T-cell acute lymphoblastic leukemia and likely acts as a haploinsufficient tumor suppressor in this leukemia (*63*). Collectively, these findings challenge the view of USP7 solely as a tumor-promoting factor, acting through the MDM2-p53 pathway. Instead, USP7 functions as a regulatory hub with multivalent effects on oncogenic and tumor suppressor networks. Thus, despite the promise of USP7 inhibitors (*2*, *10*, *18*), further dissection of the USP7 molecular network will be crucial to instruct their potential therapeutic use.

Here, we have focused on the role of USP7 in Polycomb regulation. USP7 modulates the ncPRC1s, particularly through stabilization of key subunits of PRC1.6. Thus, depending on the relative cellular levels of various PRC1s, the impact of USP7 on H2AK119ub1 might vary between distinct cell types or at different developmental stages. USP7 has a remarkable range of interaction partners (Fig 1E), of which only a portion appears to be stabilized by USP7 (Fig. 3). Future studies will address the relevance of these other USP7 partners. Deubiquitylation of USP7 substrates might regulate functional properties, without affecting protein stability. Conversely, USP7-binding proteins might direct its recruitment or modulate its activity, similar to guanosine monophosphate synthase (*4*, *9*, *64*, *65*). Our identification of protein and transcriptional targets of USP7 provides a roadmap for future analysis of its role in (neuro)development and cancer.

MATERIALS AND METHODS

Cloning procedures

Full-length cDNAs encoding USP7, USP7-C223S, PCGF1-6, and USP7-interacting proteins were cloned into pENTR11 (Invitrogen). Vectors that express enhanced GFP (eGFP)–fusion proteins were generated by recombining coding sequences into destination vectors pCS-eGFP-DEST or pCS-Cherry-DEST using LR Clonase II–mediated recombination. pDEST-3xFLAG was constructed from pCS-eGFP-DEST by replacing the GFP coding sequence with 3xFLAG using the Age I and Bgl II restriction sites. This vector was used to generate the pDEST-3xFLAG-PCeGF1-6 plasmids. All other Flag-tagged constructs were made in either pLX302 or a gateway-compatible version of pQCXIP (Promega; pQCXIP-DEST) after engineering a 3xFLAG-tag in the corresponding pENTR11 clones. CRISPR constructs were made in pSPCas9(BB)-2A-Puro (PX459) V2.0, using the Bbs I restriction sites, or in pLentiCRISPRv2GFP, using Esp3 I restriction sites. The pTRE3GBI_eGFP plasmid was constructed by inserting eGFP using the Eco RI and Kpn I restriction site. The full-length cDNA encoding Ring1A was cloned into the pTRE3GBI_eGFP using Kpn I and Pst I restriction sites. The Ring1A mutants I50S and C72A were produced by site-directed mutagenesis PCR. The RING1B-dTAG construct was made in pLEX_305-N-dTAG (Addgene, plasmid #91797). The integrity of all constructs that we generated was verified by DNA sequencing of the entire coding sequence and flanking regions. See table S1 for an overview of all plasmids.

Cell culture

HEK293T and U2OS cells were cultured in Dulbecco's modified Eagle's medium (DMEM; Gibco) supplemented with 10% fetal bovine serum (FBS) and a combination of penicillin (100 units/ml) and streptomycin (100 μg/ml; 1% Pen/Strep). DLD1 and HCT116 cells were cultured in RPMI 1640 (Gibco), 10% FBS, and 1% Pen/Strep. Culture medium for DLD1 RING1A/B-DKO cells with stable integration of pTRE3GBI-eGFP-Ring1A WT/I50S/C72A or pLEX_305-N-dTAG-Ring1B was supplemented with G-418 DiSulphate (200 μg/ml; G418; Formedium) or puromycin (3.3 μg/ml; Invitrogen), respectively. HAP1 cells were cultured in Iscove's modified Dulbecco's medium (Gibco) supplemented with 10% FBS and 1% Pen/Strep. All cells were maintained at 37°C in a humidified incubator with 5% CO_2. Typically, cultures were split at 80% confluency (~1 × 10^7 cells per 10-cm dish). Medium was aspirated, and cells were washed quickly with phosphate-buffered saline [PBS; 137 mM NaCl, 2.7 mM KCl, 10 mM Na_2HPO_4, and 1.8 mM KH_2PO_4 (pH7.4)] at 37°C, which was aspirated and replaced with PBS containing 0.05% trypsin and 0.53 mM EDTA. Following cell detachment, medium with FBS was added, and cells were resuspended and split. All cell lines were routinely checked for mycoplasma.

Generation of cell lines

HAP1-RING1B-KO, HAP1-RING1A/B-KO U2OS-USP7-KO, and DLD1-RING1A/B-DKO were generated by CRISPR-Cas9–nickase–mediated genome editing. Oligonucleotides encoding the forward and reverse guide RNAs (see table S1) were annealed, phosphorylated, and ligated into either pSpCas9(Bb)-2APuro px459 v2, linearized with Bbs I, or pLentiCRISPRv2-GFP, linearized with Esp3 I. To generate HAP1-RING1B-KO and HAP1-RING1A/B-KO cell lines, HAP1 and HAP1-RING1A/B-KO cells were seated in six-well plates and transfected with a combination of pX459-RING1B-guide1, pX459-RING1B-guide3, and pLentiCRISPRv2-GFP_ScRING1B (2.5-μg total DNA per well). Using polyethylenimine (PEI; at a DNA:PEI ratio of 1:3) 48 hours after transfection, high GFP-positive single cells were sorted by fluorescence-activated cell sorting into 96-well plates and cultivated until colonies were obtained. After

10 days, clones were duplicated and screened for the absence of RING1B by immunoblotting. The same protocol was used to generate DLD-RING1A/B DKO cells, with the modification that DLD1-WT cells were transfected with a mixture of pLentiCRISPR.V2-GFP_SCRing1A, pLentiCRISPR.V2-GFP_Ring1AGecko1 pX459-RING1B-guide1, pX459-RING1B-guide 3, and pLentiCRISPRv2-GFP_ScRING1B (2.5-μg total DNA per well). For all cell lines, the absence of RING1A and/or RING1B was verified by mass spectrometric analysis. To generate U2OS-USP7-KO cells, U2OS cells were seated in six-well plates and transfected with pX459-USP7-guide 2 using FuGENE 6 (Promega), according to the manufacturer's protocol. After 18 hours, the medium was replaced with fresh medium. Following 24-hour recovery, cells were grown in the presence of puromycin (1 μg/ml). To prevent plasmid integration, puromycin was removed after 3 days and monoclonal colonies were grown, isolated, and expanded. USP7 KO lines were first identified by immunoblotting. The absence of USP7 was verified by mass spectrometric analysis. The Dox-inducible cell lines DLD1-KO-Dox-USP7 and DLD1-RING1A/B DKO-Dox-Ring1A-wt/I50S/C72A were generated by transfection of DLD1-USP7-KO or DLD1-RING1A/B-DKO cells with either pTRE3G-BI-eGFP-USP7, pTRE3G-BI-eGFP-RING1A, pTRE3G-BI-eGFP-RING1A-I50S, or pTRE3G-BI-eGFP-RING1A-C72A, together with the Tet-ON pEF1α-Tet3G plasmid. Plasmids were linearized with Bsa I. Cells were transfected in six-well plates with 1.5 μg of total plasmid DNA per well using FuGENE HD Transfection Reagent (Promega) according to the manufacturer's instructions. After 3 days, the cells were split into two 10-cm dishes in RPMI, 10% FBS, and 1% Pen/Strep containing Dox (1 μg/ml) and G418 (400 μg/ml). Monoclonal cell colonies expressing the transgene were selected by fluorescence microscopy, isolated, and used to establish stable cell lines. Homogeneous expression of the GFP-fusion proteins in all cells was verified by fluorescence microscopy. Cell lines were maintained on G418 (200 μg/ml). Transgene expression was induced with Dox (1 μg/ml). To generate DLD1-DKO-dTAG-RING1B, DLD1-RING1A/B-KO cells were transfected with pLEX_305-N-dTAG-Ring1B plasmid linearized with Sca1. DLD1-RING1A/B-KO cells were transfected in six-well plates with 1.5 μg of total plasmid DNA per well using FuGENE HD Transfection Reagent according to the manufacturer's instructions. After 3 days, the cells were split into two 10-cm dishes in RPMI, 10% FBS, and 1% Pen/Strep containing puromycin (3.3 μg/ml). Monoclonal cell colonies were picked and checked for transgene expression and responsiveness to 500 nM dTAG13 (Sigma-Aldrich; SML2601) by Western blot analysis. The cell lines were maintained on puromycin (3.3 μg/ml).

Antibody production

We cloned cDNAs into pGEX-2TKN; glutathione *S*-transferase (GST) fusion proteins were then expressed in BL21 *Escherichia coli*, purified, and used for antibody production by immunization with GST fused to the following polypeptides: BAF155, amino acids 742 to 1071 (rabbit); full-length cherry (rabbit); SCML2, amino acids 20 to 395 (guinea pig); and USP11, amino acids 1 to 306 (rabbit).

Cell collection and immunoblotting

Medium was removed by aspiration; cells were washed with ice-cold PBS, aspirated, and scraped loose in 10 ml of ice-cold PBS and transferred to a 15-ml centrifuge tube. Cells were recovered by centrifugation at 1000*g* for 5 min. Following aspiration, cell pellets were snap-frozen in liquid nitrogen and stored at −80°C. Thawed cell pellets were resuspended in ~0.5 ml (per 10-cm^2 dish) of 1× Laemmli buffer [63 mM tris-HCl (pH 6.8), 0.0005% bromophenol blue, 10% glycerol, and 2% SDS, containing 0.1 M dithiothreitol (DTT)]. Following brief sonication (four to five rounds of 30-s on/off cycle at high setting) in a Bioruptor UCD-200 sonicator (Diagenode), samples were boiled for 4 min, cleared by centrifugation, and transferred to a fresh Eppendorf tube. Equivalent amounts of sample were analyzed by SDS–polyacrylamide gel electrophoresis (SDS-PAGE) followed by immunoblotting (described below). For acid extraction of histones, cells grown on a 10-cm dish were harvested as described above. The cell pellet was then resuspended in 200 μl of PBST (PBS containing 0.5% Triton X-100 and 0.2 mM phenylmethanesulfonyl fluoride). Samples were left on ice for 10 min, collected by centrifugation in an Eppendorf centrifuge at 2000 rpm for 10 min, and aspirated. Cells were resuspended and washed one more time with PBST, collected by centrifugation, and aspirated. Cell pellets were resuspended in 200 μl of 0.2 M HCl and sonicated in a Bioruptor UCD-200 sonicator for five 30-s bursts, followed by overnight extraction at 4°C. Next, samples were centrifuged for 10 min at maximum speed, and the supernatant was transferred to a new Eppendorf tube. Samples were neutralized by the addition of 1/10th volume 2 M NaOH (~20 μl). Following SDS-PAGE on a Bio-Rad Mini-PROTEAN system, proteins were transferred to nitrocellulose membrane (Amersham Protran pore sizes, 0.2 or 0.45 μm). Membranes were blocked in 10% (w/v) skimmed milk in PBS-Tween [PBS and 0.1% (w/v) Tween 20] for at least 30 min at room temperature and then incubated with primary antibody [diluted in PBS containing 3% bovine serum albumin (BSA) (w/v)] overnight at 4°C. Membranes were washed several times with PBS/Tween and then incubated with alkaline phosphatase–conjugated secondary antibodies (diluted in PBS-Tween 3% BSA). Following a series of washes with PBS/Tween, blots were developed using alkaline phosphatase chromogenic nitro blue tetrazolium/5-bromo-4-chloro-indolyl phosphate detection. Primary and secondary antibodies are listed in table S1.

Cell collection for immunopurification and mass spectrometric analysis

For IP of Flag-tagged proteins, two 15-cm dishes of HEK293T cells (grown at ~70% confluency) were transfected with the appropriate expression vectors. Medium was replaced with FBS-free DMEM, and cells were transfected with 20 μg of expression vector DNA per 15-cm dish using PEI at a DNA:PEI ratio of 1:3. After 16 hours, the medium was replaced with DMEM containing 10% serum. Twenty-four hours later, cells were collected by scraping in PBS as described above, but after collection by centrifugation, cells were resuspended in ice-cold PBS, pooled, washed by inversion for a few minutes, and then collected by centrifugation. The PBS wash step was repeated one more time, and then, cell pellets were aspirated, snap-frozen in liquid nitrogen, and stored at −80°C. Biological triplicates of DLD1 WT, DLD1-USP7-KO, and DLD1-KO-Dox-USP7 cells were grown in 10-cm plates at ~8 × 10^6 cells per plate. GFP-USP7 expression in DLD1-KO-Dox-USP7 cells was induced by the addition of Dox (1 μg/ml) for 24 hours, 3 days, or 9 days (+Dox). Cells were harvested by trypsinization, washed 2× with PBS, aspirated, snap-frozen in liquid nitrogen, and stored at −80°C.

Immunopurification

All procedures were on ice or at 4°C. Cell pellets were resuspended in 1 ml of NEH buffer [10% glycerol, 5 mM EDTA, 150 mM NaCl, 50 mM Hepes-KOH (pH 7.6), 0.1% NP-40, and 1.5 mM $MgCl_2$] and

a cocktail of protease inhibitors: 1 μM pepstatin, 1 μM aprotinin, and 1 μM leupeptin, followed by sonication for 5 min using a 30-s on/off cycle. Next, Benzonase (Novagen) was added to the lysates to a final concentration of 100 U/ml, followed by incubation of a rotating wheel for 30 min at 4°C. After addition of ethidium bromide to a final concentration of 50 μg/ml, the lysate was cleared by centrifugation at 20,000*g* for 20 min, and the supernatant was transferred to a clean 1.5-ml Eppendorf tube. The day before use, anti-Flag M2 agarose (Sigma-Aldrich) were washed 3× with PBS followed by one wash with 0.1 M glycine (pH 3.5) and 150 mM NaCl. Next, the anti-Flag agarose was washed three times with PBS, and antibodies were renatured by incubation overnight in PBS at 4°C. The next morning, the Flag agarose was equilibrated with NEH buffer, and 60 μl of slurry (corresponding to 20 μl of packed beads) was added to 1 ml of WCE, followed by 2.5-hour incubation on a rotating wheel at 4°C. Next, the anti-Flag agarose was washed seven times with HEG/150/0.1% NP-40 [50 mM Hepes KOH (pH 7.6), 1.5 mM EDTA, 10% glycerol, containing 150 mM NaCl, 0.1% NP40, and a cocktail of protease inhibitors: 1 μM pepstatin, 1 μM aprotinin, and 1 μM leupeptin], two times with HEG/150/0.01% NP-40, and lastly two times with HEG/100. The resulting immunopurified proteins on beads were directly processed for mass spectrometric analysis.

Interactomics and global proteomics

Immunopurified proteins were subjected to reduction with dithiothreitol and alkylation with iodoacetamide and digested on beads with trypsin (sequencing grade; Promega). For global proteome analysis of WCEs, cells were lysed in 100 mM tris/HCl (pH 8.2), containing 1% sodium deoxycholate (SDC) using sonication in a Bioruptor Pico (Diagenode). Protein concentrations were measured using the bicinchoninic acid assay (Thermo Fisher Scientific). Protein (100 μg) was reduced in lysis buffer with 5 mM dithiothreitol and alkylated with 10 mM iodoacetamide. Next, proteins were digested with 2.5 μg of trypsin (1:40 enzyme:substrate ratio) overnight at 37°C. After digestion, peptides were acidified with trifluoroacetic acid (TFA) to a final concentration of 0.5% and centrifuged at 10,000*g* for 10 min to spin down the precipitated SDC. Peptides dissolved in the supernatant were desalted on a 50 mg of C18 Sep-Pak cartridge (Waters). After washing the cartridge with 0.1% TFA, peptides were eluted with 50% acetonitrile and dried in a SpeedVac centrifuge.

Nanoflow LC-MS

Mass spectrometry analyses were essentially performed as described (*66*). Briefly, proteolytic peptides were analyzed by nLC-MS/MS on an EASY-nLC coupled to an Orbitrap Lumos Tribrid mass spectrometer (Thermo Fisher Scientific) operating in positive mode. Peptides were trapped on a 2 cm–by–100 μm PepMap C18 column (Thermo Fisher Scientific, 164564) and then separated on an in-house packed 25 cm–by–75 μm capillary column with 1.9-μm ReproSil-Pur C18 beads (Maisch) at a flow rate of 250 nl/min using a linear gradient of 0 to 32% acetonitrile in 0.1% formic acid during 90 min. The eluate was directly sprayed into the electrospray ionization source of the mass spectrometer. Spectra were acquired according to a data-dependent acquisition regime in continuum mode. Spectra were recorded in the Orbitrap at 120,000 resolution for MS1 and 30,000 resolution for MS2 in profile mode, with standard AGC target settings. Fragmentation of the peptides was performed by HCD. For targeted proteomics, a PRM regime was used to select for a set of previously selected peptides on an Orbitrap Eclipse Tribrid mass spectrometer (Thermo Fisher Scientific) operating in positive mode and running Tune version 3.3. Precursors were selected in the quadrupole with an isolation width of 0.7 mass/charge ratio and fragmented with HCD using 30% collision energy. MS1 and MS2 spectra were recorded in the Orbitrap at 30,000 resolution in profile mode, with standard AGC target settings. The injection time mode was set to dynamic with a minimum of nine points across the peak. The sequence of sampling was blanks first and then in order of increasing peptide input amounts to avoid any contamination of previous samples.

Mass spectrometry data analysis

USP7 interactomics mass spectrometry data were analyzed using MaxQuant v1.6.0.16 (www.maxquant.org) with standard settings and with the additional options "LFQ" and "iBAQ" selected. Fragment was set to 20 parts per million (ppm). Raw mass spectrometry data recorded on the Orbitrap Eclipse with the FAIMS option were first converted into mzXML format using the FAIMS MzXML generator software tool (https://coonlabs.com/) before MaxQuant analysis. An FDR of 0.01 for proteins and peptides and a minimum peptide length of seven amino acids were set. The Andromeda search engine was used to search the MS/MS spectra against the UniProt database (taxonomy: *Homo sapiens*, release September 2017) concatenated with the reversed versions of all sequences. A maximum of two missed cleavages was allowed. The peptide tolerance was set to 10 ppm, and the fragment ion tolerance was set to 0.6 Da for HCD spectra. The enzyme specificity was set to trypsin, and cysteine carbamidomethylation was set as a fixed modification, while STY phosphorylation was set as a variable modification. Both the PSM and protein FDR were set to 0.01. In case the identified peptides of two proteins were the same or the identified peptides of one protein included all peptides of another protein, these proteins were combined by MaxQuant and reported as one protein group. Before further statistical analysis, known contaminants and reverse hits were removed. MaxQuant output data were further analyzed using Perseus (https://www.maxquant.org/perseus/). The proteingroups.txt output table was first filtered for contaminants, reverse hits, and proteins based on only one tryptic peptide. For the identification of bona fide interactors, *t* test–based statistics was applied on iBAQ data. First, iBAQ data were $\log_2$-transformed, and for the generation of volcano plots, missing values were imputed by normal distribution (width = 0.3 and shift = 1.8). For all other analyses, only proteins with at least three valid values over all eight samples (i.e., five controls and three IP samples, except for PCGF3, for which only two IPs were available) were taken into account. Statistical outliers for the target protein IP data compared to controls were determined using a two-sample two-tailed *t* test. Multiple testing correction was applied by using a permutation-based FDR method. PRM data were analyzed with Skyline (https://skyline.ms/). Skyline reports containing all essential data such as area per fragment for each target were loaded into R and manually curated. If the expected peptide fragment ion peaks could not be correctly assigned, fragments were excluded, and their associated areas were set to 0. Summed areas were calculated for all fragment ion peak chromatograms for each target peptide and then summed over all targeted peptides per protein. SDs (three biological and two technical replicates) were calculated for every target peptide in each condition and indicated in the bars. All summed areas were normalized to the WT condition. Peptide bar graphs were constructed by dividing the bar for each target peptide into the respective areas

for every fragment ion peak. For the protein abundance comparison between WT and KO conditions, the normalized areas for all detected fragment ion chromatograms were summed over all selected target peptides per protein and visualized in box plots. The median for the WT condition was set to 1. Protein abundances are based on two or more target tryptic peptides unless indicated otherwise. Proteins for which no peptides were detected in a specific condition are indicated by an asterisk.

Cotransfection experiments

To test whether stabilization of potential target proteins by USP7 is dependent on its deubiquitylation activity, U2OS-USP7-KO cells were cotransfected with vectors encoding GFP- or mCherry-tagged substrates, combined with vectors expressing Flag-USP7, Flag-USP7-C223S, or empty vector (table S1). Cells were seeded in six-well plates and transfected the following day with PEI according to standard procedures. Typically, 2 to 2.5 μg of DNA was mixed with 6 μg of PEI in a total volume of 200 μl of PBS. Culture medium was replaced with FBS-free DMEM medium, and the transfection mix was added. The next day, the medium was replaced with complete DMEM containing 10% FBS. Twenty-four hours later, the medium was removed by aspiration and cells were washed once with PBS and then collected by scraping in PBS. The cell suspension was centrifuged at 2000*g*, aspirated, and resuspended in 200 μl of radioimmunoprecipitation assay lysis buffer [50 mM tris HCl (pH 7.4), 150 mM NaCl, 1.0% NP-40, 0.5% SDC, 1.0 mM EDTA, and 0.1% SDS] supplemented with 1 mM DTT and protease inhibitors pepstatin A (1 μl/ml), leupeptin (1 μg/ml), aprotinin (1 μg/ml), and 0.2 mM 4-(2-aminoethyl)benzenesulfonyl fluoride hydrochloride (AEBSF). Samples were sonicated for 5 min on a 30-s on/30-s off cycle in a Bioruptor UCD-200 sonicator to shear chromosomal DNA. Samples were analyzed by immunoblotting.

Real-time quantitative PCR

Biological triplicates of Dld1 and HAP1 cell lines were grown in six-well plates till ~80% confluence, and RNA was extracted using TRI-reagent (Sigma-Aldrich) according to the manufacturer's protocol. Expression of GFP-RING1A, GFP-RING1A-I50S, or GFP-RING1A-C72A was induced with Dox (1 μg/ml) for 6 days before RNA isolation. RNA levels were analyzed by first-strand cDNA synthesis using Oligo(dT) and Superscript II reverse transcriptase (Invitrogen) and subsequent qPCR with SYBR green I and platinum Taq DNA polymerase (Invitrogen) using the CFX96 Touch Real-Time PCR System (Bio-Rad). Analysis was performed using the $2^{-\Delta\Delta C(T)}$ method. *TBP* was used for normalization.

RNA isolation, sequencing, and analysis

Biological triplicates of DLD1 WT, DLD1-USP7-KO, and DLD1-KO-Dox-USP7 were grown in 10-cm^2 plates. GFP-USP7 expression was induced by the addition of Dox (1 μg/ml) for 24 hours, 3days, or 9 days (+Dox). For RNA isolation, the medium was removed, and 3 ml of TriPure isolation reagent (Roche) was added directly onto the cells. Cell lysate (1 ml) was transferred to a 1.5-ml Eppendorf tube and left to incubate for 5 min at room temperature. Next, 0.2 ml of chloroform was added, shaken vigorously, and left for 15 min at room temperature. Samples were centrifuged for 15 min at 12,000*g* at 4°C. The aqueous phase was transferred to a fresh tube, and 0.5 ml of isopropanol was added, mixed, and incubated for 10 min at room temperature, followed by centrifugation at 12,000*g* at 4° for 10 min. The precipitated RNA pellet was washed two times with 75% ethanol, air-dried, and resuspended in 125 μl of nuclease-free water. All samples were prepped with the Illumina TruSeq Stranded mRNA Library Prep Kit. The resulting cDNA libraries were sequenced according to the Illumina Truseq Rapid V2 protocol on an Illumina HiSeq2500 sequencer. FASTQ files were aligned against the human reference genome (hg19) using HiSat2 (version 2.1.0; 84), and mapped reads were assigned to RNAs using HTSeq count with the following settings: -m union -s reverse -t exon. DESeq2 (bioconductor.org) was used to normalize for library size, and normalized reads were further corrected for batch variation between independent experiments using the SVA R package (bioconductor.org). Batch-corrected values were used in DESeq2 for differential gene expression analysis. Genes were considered differentially expressed if they fulfilled the following conditions: normalized $\log_2$ read counts ≥ 5, fold change ≥ 2, and FDR < 0.05 at one or more time points. GO term enrichment analysis of differentially expressed genes was performed by DAVID (https://david.ncifcrf.gov/) and Metascape (metascape.org). Only Gene Ontology terms enriched with FDR <0.05 were considered significant.

Chromatin IP with reference exogenous genome

Biological duplicates of DLD1 WT, DLD1-DKO-Dox-RING1A, DLD1-KO-Dox-USP7, HAP1 WT, and HAP1 RING1A/B-KO cells were grown in two 15-cm dishes per condition, which were processed independently. GFP-USP7 or GFP-RING1A expression was induced by addition of Dox (1 μg/ml) for 3 days (+Dox). Two other plates were mock-treated (−Dox). Cells were harvested by trypsinization, followed by cell counting. For cross-linking, 17 million cells were suspended in 10 ml of PBS. Cells were fixed by the addition of 1% formaldehyde and incubation on a roller mixer for 10 min. Fixation was stopped by the addition of glycine (125 mM). Next, cells were washed twice with PBS and lysed in 1 ml of lysis buffer: 50 mM tris-HCl (pH 8.0), 10 mM EDTA, and 1% SDS, supplemented with protease inhibitors pepstatin A (1 μl/ml), leupeptin (1 μg/ml), aprotinin (1 μg/ml), and 0.2 mM AEBSF. These protease inhibitors were present in all subsequent buffers until elution. Cross-linked chromatin was sheared to approximately 200–base pair (bp) DNA length in a Bioruptor Pico sonication system. The normalization reference exogenous genome was isolated from ~80 million *Drosophila* S2 cells (one 15-cm^2 dish). Fixation was performed as above with 1% formaldehyde in PBS for 10 min. S2 cells were lysed in 1.2 ml of 0.75% SDS, 10 mM EDTA, and 50 mM tris-HCl (pH 8.0), supplemented with protease inhibitors. *Drosophila* chromatin was sheared to 200- to 300-bp DNA length. DLD1-KO-Dox-USP7 chromatin (180 μl) was combined with 20 μl of S2 chromatin and diluted 10-fold with dilution buffer [20 mM tris (pH 8.0), 1% Triton X-100, 2 mM EDTA, and 150 mM NaCl], cleared by centrifugation at 15,000*g* for 20 min. The supernatant was transferred to a fresh tube and incubated overnight at 4°C in the presence of either 10 μl of anti-H3K27me3 (Cell Signaling Technology, #9733) or 5 μl of anti-H2AK119ub1 (Cell Signaling Technology, #8240) on a rotating wheel. The next morning, 50 μl of Dynabeads protein A slurry (Invitrogen), which was blocked overnight with 1% BSA in dilution buffer, was added, followed by a 3-hour incubation. Next, beads were washed four times with wash buffer [20 mM tris-HCl (pH 8.0), 2 mM EDTA, 0.1% SDS, and 1% Triton X-100] containing 150 mM NaCl, followed once with wash buffer containing 500 mM NaCl. DNA was eluted with 0.1 M $NaHCO_3$, 1% SDS, and proteinase K

(0.5 mg/ml) for 2 hours at 37°C, followed by an overnight incubation at 65°C. DNA was subsequently purified by double phenol/chloroform extraction, followed by ethanol precipitation. ChIP-Rx-seq libraries were prepared using the ThruPLEX DNA-Seq Kit (Takara Bio, R400675), according to the manufacturer's instructions. ChIP-Rx DNA was repaired to obtain blunt-ended double-stranded DNA followed by ligation of stem-loop adapters. The stem loop was cleaved off, and a library amplification was performed that extended the template with dual indices and sequence needed for posterior sequencing on an Illumina HiSeq 2500 sequencer (dual-indexed 50-bp paired-end reads).

ChIP-Rx-seq data analysis

FASTQ files were mapped against human genome (hg19) and *Drosophila* genome (Dm6) using Bowtie 2 (bowtie-bio.sourceforge.net) and default parameters. SAM files were further filtered for uniquely mapped reads and high-quality mapping (-q 10) using SAMtools, and PCR duplicates were removed using MarkDuplicates in PICARD tools. For ChIP-Rx, total reads in *Drosophila* BAM files were used to calculate the spike-in normalization factors and were used for downscaling the corresponding human BAM files as described (*49*). Normalized human BAM files were further downscaled on the basis of the BAM file with the lowest total read counts to normalize for sequencing depth. Next, BAM files were converted to BED files using BEDTools, and reads were extended by 160 nt and converted to BedGraph using bamCoverage tool from the deepTools suite. BedGraphs were converted to BigWig files using bedGraphToBigWig from UCSC tool suite for further visualization using Integrative Genomics Viewer browser.

ChIP-Rx-seq peak calling and analysis

H3K27me3 and H2AK119ub1 peaks were called by using SICER (*50*) with default settings and a window size of 200 bp and a gap size of 600 bp. Peaks overlapping with human blacklist regions were excluded using BEDTools. Only peaks that were detected in both replicates of a biological group (peaks showing ≥1-bp overlap) were selected. Peaks across different biological groups were then compiled and merged if they were within a 5-kb window to generate the final set of peaks. Reads counting within peaks was carried out using BEDTools intersect and normalized BAM files. To assign ChIP peaks to corresponding promoters, BEDTools window was used and promoters within 1-kb distance to H3K27me3- or H2AK119Ub peaks were selected. For closest gene analysis, BEDTools closest was used, and the closest promoters to H3K27me3 or H2AK119Ub were selected. Promoters were determined as ±1 kb of transcription start sites. Biofluff 3.0.4 (https://fluff.readthedocs.io) was used for heatmap analysis with the following parameters: -e 5000 -F 250 -m -S. For average plots, read counts were generated by Biofluff in 25-bp windows in selected peaks or promoters, further averaged across all regions, and visualized with R. GO term enrichment analysis of genes associated with H3K27me3 or H2AK119Ub was performed by DAVID (https://david.ncifcrf.gov/) and Metascape (metascape.org). Only GO terms enriched with FDR <0.05 were considered significant.

SUPPLEMENTARY MATERIALS

Supplementary material for this article is available at https://science.org/doi/10.1126/sciadv.abq7598

View/request a protocol for this paper from *Bio-protocol*.

REFERENCES AND NOTES

1. R. Q. Kim, T. K. Sixma, Regulation of USP7: A high incidence of E3 complexes. *J. Mol. Biol.* **429**, 3395–3408 (2017).
2. R. Rawat, D. T. Starczynowski, P. Ntziachristos, Nuclear deubiquitination in the spotlight: The multifaceted nature of USP7 biology in disease. *Curr. Opin. Cell Biol.* **58**, 85–94 (2019).
3. A. Bojagora, V. Saridakis, USP7 manipulation by viral proteins. *Virus Res.* **286**, 198076 (2020).
4. J. A. van der Knaap, B. R. Kumar, Y. M. Moshkin, K. Langenberg, J. Krijgsveld, A. J. Heck, F. Karch, C. P. Verrijzer, GMP synthetase stimulates histone H2B deubiquitylation by the epigenetic silencer USP7. *Mol. Cell* **17**, 695–707 (2005).
5. N. Kon, Y. Kobayashi, M. Li, C. L. Brooks, T. Ludwig, W. Gu, Inactivation of HAUSP in vivo modulates p53 function. *Oncogene* **29**, 1270–1279 (2010).
6. Y.-H. Hao, M. D. Fountain Jr., K. Fon Tacer, F. Xia, W. Bi, S. H. Kang, A. Patel, J. A. Rosenfeld, C. Le Caignec, B. Isidor, I. D. Krantz, S. E. Noon, J. P. Pfotenhauer, T. M. Morgan, R. Moran, R. C. Pedersen, M. S. Saenz, C. P. Schaaf, P. R. Potts, USP7 acts as a molecular rheostat to promote WASH-dependent endosomal protein recycling and is mutated in a human neurodevelopmental disorder. *Mol. Cell* **59**, 956–969 (2015).
7. M. D. Fountain, D. S. Oleson, M. E. Rech, L. Segebrecht, J. V. Hunter, J. M. McCarthy, P. J. Lupo, M. Holtgrewe, R. Moran, J. A. Rosenfeld, B. Isidor, C. Le Caignec, M. S. Saenz, R. C. Pedersen, T. M. Morgan, J. P. Pfotenhauer, F. Xia, W. Bi, S. L. Kang, A. Patel, I. D. Krantz, S. E. Raible, W. Smith, I. Cristian, E. Torti, J. Juusola, F. Millan, I. M. Wentzensen, R. E. Person, S. Küry, S. Bézieau, K. Uguen, C. Férec, A. Munnich, M. van Haelst, K. D. Lichtenbelt, K. van Gassen, T. Hagelstrom, A. Chawla, D. L. Perry, R. J. Taft, M. Jones, D. Masser-Frye, D. Dyment, S. Venkateswaran, C. Li, L. F. Escobar, D. Horn, R. C. Spillmann, L. Peña, J. Wierzba, T. M. Strom, I. Parenti, F. J. Kaiser, N. Ehmke, C. P. Schaaf, Pathogenic variants in USP7 cause a neurodevelopmental disorder with speech delays, altered behavior, and neurologic anomalies. *Genet. Med.* **21**, 1797–1807 (2019).
8. C. L. Brooks, M. Li, M. Hu, Y. Shi, W. Gu, The p53—Mdm2—HAUSP complex is involved in p53 stabilization by HAUSP. *Oncogene* **26**, 7262–7266 (2007).
9. B. A. Reddy, J. A. van der Knaap, A. G. Bot, A. Mohd-Sarip, D. H. Dekkers, M. A. Timmermans, J. W. Martens, J. A. Demmers, C. P. Verrijzer, Nucleotide biosynthetic enzyme GMP synthase is a TRIM21-controlled relay of p53 stabilization. *Mol. Cell* **53**, 458–470 (2014).
10. P. Li, H. M. Liu, Recent advances in the development of ubiquitin-specific-processing protease 7 (USP7) inhibitors. *Eur. J. Med. Chem.* **191**, 112107 (2020).
11. A. Georges, E. Marcon, J. Greenblatt, L. Frappier, Identification and characterization of USP7 targets in cancer cells. *Sci. Rep.* **8**, 15833 (2018).
12. M. Steger, V. Demichev, M. Backman, U. Ohmayer, P. Ihmor, S. Müller, M. Ralser, H. Daub, Time-resolved in vivo ubiquitinome profiling by DIA-MS reveals USP7 targets on a proteome-wide scale. *Nat. Commun.* **12**, 5399 (2021).
13. G. N. Maertens, S. El Messaoudi-Aubert, S. Elderkin, K. Hiom, G. Peters, Ubiquitin-specific proteases 7 and 11 modulate Polycomb regulation of the INK4a tumour suppressor. *EMBO J.* **29**, 2553–2565 (2010).
14. E. Lecona, V. Narendra, D. Reinberg, USP7 cooperates with SCML2 to regulate the activity of PRC1. *Mol. Cell. Biol.* **35**, 1157–1168 (2015).
15. Z. Gao, J. Zhang, R. Bonasio, F. Strino, A. Sawai, F. Parisi, Y. Kluger, D. Reinberg, PCGF homologs, CBX proteins, and RYBP define functionally distinct PRC1 family complexes. *Mol. Cell* **45**, 344–356 (2012).
16. R. Liefke, V. Karwacki-Neisius, Y. Shi, EPOP interacts with elongin BC and USP7 to modulate the chromatin landscape. *Mol. Cell* **64**, 659–672 (2016).
17. D. Su, W. Wang, Y. Hou, L. Wang, X. Yi, C. Cao, Y. Wang, H. Gao, Y. Wang, C. Yang, B. Liu, X. Chen, X. Wu, J. Wu, D. Yan, S. Wei, L. Han, S. Liu, Q. Wang, L. Shi, L. Shan, Bimodal regulation of the PRC2 complex by USP7 underlies tumorigenesis. *Nucleic Acids Res.* **49**, 4421–4440 (2021).
18. H. Maat, T. J. Atsma, S. M. Hogeling, A. Rodríguez López, J. Jaques, M. Olthuis, M. P. de Vries, C. Gravesteijn, A. Z. Brouwers-Vos, N. van der Meer, S. Datema, J. Salzbrunn, G. Huls, R. Baas, J. H. A. Martens, V. van den Boom, J. J. Schuringa, The USP7-TRIM27 axis mediates non-canonical PRC1.1 function and is a druggable target in leukemia. *iScience* **24**, 102435 (2021).
19. B. Schuettengruber, H. M. Bourbon, L. Di Croce, G. Cavalli, Genome regulation by Polycomb and trithorax: 70 years and counting. *Cell* **171**, 34–57 (2017).
20. A. P. Bracken, G. L. Brien, C. P. Verrijzer, Dangerous liaisons: Interplay between SWI/SNF, NuRD, and Polycomb in chromatin regulation and cancer. *Genes Dev.* **33**, 936–959 (2019).
21. A. Piunti, A. Shilatifard, The roles of Polycomb repressive complexes in mammalian development and cancer. *Nat. Rev. Mol. Cell Biol.* **22**, 326–345 (2021).
22. A. R. Pengelly, Ö. Copur, H. Jäckle, A. Herzig, J. Müller, A histone mutant reproduces the phenotype caused by loss of histone-modifying factor Polycomb. *Science* **339**, 698–699 (2013).
23. J. R. Yu, C. H. Lee, O. Oksuz, J. M. Stafford, D. Reinberg, PRC2 is high maintenance. *Genes Dev.* **33**, 903–935 (2019).
24. M. de Napoles, J. E. Mermoud, R. Wakao, Y. A. Tang, M. Endoh, R. Appanah, T. B. Nesterova, J. Silva, A. P. Otte, M. Vidal, H. Koseki, N. Brockdorff, Polycomb group

proteins Ring1A/B link ubiquitylation of histone H2A to heritable gene silencing and X inactivation. *Dev. Cell* **7**, 663–676 (2004).
25. H. Wang, L. Wang, H. Erdjument-Bromage, M. Vidal, P. Tempst, R. S. Jones, Y. Zhang, Role of histone H2A ubiquitination in Polycomb silencing. *Nature* **431**, 873–878 (2004).
26. S. Tamburri, E. Conway, D. Pasini, Polycomb-dependent histone H2A ubiquitination links developmental disorders with cancer. *Trends Genet.* **38**, 333–352 (2021).
27. S. Hauri, F. Comoglio, M. Seimiya, M. Gerstung, T. Glatter, K. Hansen, R. Aebersold, R. Paro, M. Gstaiger, C. Beisel, A high-density map for navigating the human Polycomb complexome. *Cell Rep.* **17**, 583–595 (2016).
28. K. Isono, T. A. Endo, M. Ku, D. Yamada, R. Suzuki, J. Sharif, T. Ishikura, T. Toyoda, B. E. Bernstein, H. Koseki, SAM domain polymerization links subnuclear clustering of PRC1 to gene silencing. *Dev. Cell* **26**, 565–577 (2013).
29. E. Seif, J. J. Kang, C. Sasseville, O. Senkovich, A. Kaltashov, E. L. Boulier, I. Kapur, C. A. Kim, N. J. Francis, Phase separation by the polyhomeotic sterile alpha motif compartmentalizes Polycomb Group proteins and enhances their activity. *Nat. Commun.* **11**, 5609 (2020).
30. A. Lagarou, A. Mohd-Sarip, Y. M. Moshkin, G. E. Chalkley, K. Bezstarosti, J. A. Demmers, C. P. Verrijzer, dKDM2 couples histone H2A ubiquitylation to histone H3 demethylation during Polycomb group silencing. *Genes Dev.* **22**, 2799–2810 (2008).
31. L. Tavares, E. Dimitrova, D. Oxley, J. Webster, R. Poot, J. Demmers, K. Bezstarosti, S. Taylor, H. Ura, H. Koide, A. Wutz, M. Vidal, S. Elderkin, N. Brockdorff, RYBP-PRC1 complexes mediate H2A ubiquitylation at Polycomb target sites independently of PRC2 and H3K27me3. *Cell* **148**, 664–678 (2012).
32. N. P. Blackledge, N. A. Fursova, J. R. Kelley, M. K. Huseyin, A. Feldmann, R. J. Klose, PRC1 catalytic activity is central to Polycomb system function. *Mol. Cell* **77**, 857–874.e9 (2020).
33. N. A. Fursova, N. P. Blackledge, M. Nakayama, S. Ito, Y. Koseki, A. M. Farcas, H. W. King, H. Koseki, R. J. Klose, Synergy between variant PRC1 complexes defines Polycomb-mediated gene repression. *Mol. Cell* **74**, 1020–1036.e8 (2019).
34. A. Scelfo, D. Fernández-Pérez, S. Tamburri, M. Zanotti, E. Lavarone, M. Soldi, T. Bonaldi, K. J. Ferrari, D. Pasini, Functional landscape of PCGF proteins reveals both RING1A/B-dependent-and RING1A/B-independent-specific activities. *Mol. Cell* **74**, 1037–1052.e7 (2019).
35. S. Tamburri, E. Lavarone, D. Fernández-Pérez, E. Conway, M. Zanotti, D. Manganaro, D. Pasini, Histone H2AK119 mono-ubiquitination is essential for polycomb-mediated transcriptional repression. *Mol. Cell* **77**, 840–856.e5 (2020).
36. N. P. Blackledge, A. M. Farcas, T. Kondo, H. W. King, J. F. McGouran, L. L. P. Hanssen, S. Ito, S. Cooper, K. Kondo, Y. Koseki, T. Ishikura, H. K. Long, T. W. Sheahan, N. Brockdorff, B. M. Kessler, H. Koseki, R. J. Klose, Variant PRC1 complex-dependent H2A ubiquitylation drives PRC2 recruitment and polycomb domain formation. *Cell* **157**, 1445–1459 (2014).
37. M. Leeb, D. Pasini, M. Novatchkova, M. Jaritz, K. Helin, A. Wutz, Polycomb complexes act redundantly to repress genomic repeats and genes. *Genes Dev.* **24**, 265–276 (2010).
38. A. R. Pengelly, R. Kalb, K. Finkl, J. Müller, Transcriptional repression by PRC1 in the absence of H2A monoubiquitylation. *Genes Dev.* **29**, 1487–1492 (2015).
39. J. A. Zepeda-Martinez, C. Pribitzer, J. Wang, D. Bsteh, S. Golumbeanu, Q. Zhao, T. R. Burkard, B. Reichholf, S. K. Rhie, J. Jude, H. F. Moussa, J. Zuber, O. Bell, Parallel PRC2/cPRC1 and vPRC1 pathways silence lineage-specific genes and maintain self-renewal in mouse embryonic stem cells. *Sci. Adv.* **6**, eaax5692 (2020).
40. I. Cohen, C. Bar, H. Liu, V. J. Valdes, D. Zhao, P. M. Galbo Jr., J. M. Silva, H. Koseki, D. Zheng, E. Ezhkova, Polycomb complexes redundantly maintain epidermal stem cell identity during development. *Genes Dev.* **35**, 354–366 (2021).
41. M. Endoh, T. A. Endo, J. Shinga, K. Hayashi, A. Farcas, K. W. Ma, S. Ito, J. Sharif, T. Endoh, N. Onaga, M. Nakayama, T. Ishikura, O. Masui, B. M. Kessler, T. Suda, O. Ohara, A. Okuda, R. Klose, H. Koseki, PCGF6-PRC1 suppresses premature differentiation of mouse embryonic stem cells by regulating germ cell-related genes. *eLife* **6**, e21064 (2017).
42. B. Stielow, F. Finkernagel, T. Stiewe, A. Nist, G. Suske, MGA, L3MBTL2 and E2F6 determine genomic binding of the non-canonical Polycomb repressive complex PRC1.6. *PLOS Genet.* **14**, e1007193 (2018).
43. H. Mathsyaraja, J. Catchpole, B. Freie, E. Eastwood, E. Babaeva, M. Geuenich, P. F. Cheng, J. Ayers, M. Yu, N. Wu, S. Moorthi, K. R. Poudel, A. Koehne, W. Grady, A. M. G. Houghton, A. H. Berger, Y. Shiio, D. MacPherson, R. N. Eisenman, Loss of MGA repression mediated by an atypical polycomb complex promotes tumor progression and invasiveness. *eLife* **10**, e64212 (2021).
44. A. M. Farcas, N. P. Blackledge, I. Sudbery, H. K. Long, J. F. McGouran, N. R. Rose, S. Lee, D. Sims, A. Cerase, T. W. Sheahan, H. Koseki, N. Brockdorff, C. P. Ponting, B. M. Kessler, R. J. Klose, KDM2B links the polycomb repressive complex 1 (PRC1) to recognition of CpG islands. *eLife* **1**, e00205 (2012).
45. J. He, L. Shen, M. Wan, O. Taranova, H. Wu, Y. Zhang, Kdm2b maintains murine embryonic stem cell status by recruiting PRC1 complex to CpG islands of developmental genes. *Nat. Cell Biol.* **15**, 373–384 (2013).
46. X. Wu, J. V. Johansen, K. Helin, Fbxl10/Kdm2b recruits polycomb repressive complex 1 to CpG islands and regulates H2A ubiquitylation. *Mol. Cell* **49**, 1134–1146 (2013).
47. Z. Gao, P. Lee, J. M. Stafford, M. von Schimmelmann, A. Schaefer, D. Reinberg, An AUTS2-polycomb complex activates gene expression in the CNS. *Nature* **516**, 349–354 (2014).
48. C. Lecerf, X. L. Bourhis, E. Adriaenssens, The long non-coding RNA H19: An active player with multiple facets to sustain the hallmarks of cancer. *Cell. Mol. Life Sci.* **76**, 4673–4687 (2019).
49. D. A. Orlando, M. W. Chen, V. E. Brown, S. Solanki, Y. J. Choi, E. R. Olson, C. C. Fritz, J. E. Bradner, M. G. Guenther, Quantitative ChIP-Seq normalization reveals global modulation of the epigenome. *Cell Rep.* **9**, 1163–1170 (2014).
50. S. Xu, S. Grullon, K. Ge, W. Peng, Spatial clustering for identification of ChIP-enriched regions (SICER) to map regions of histone methylation patterns in embryonic stem cells. *Methods Mol. Biol.* **1150**, 97–111 (2014).
51. F. Chiacchiera, A. Rossi, S. G. Jammula, A. Piunti, A. Scelfo, P. Ordóñez-Morán, J. Huelsken, H. Koseki, D. Pasini, Polycomb complex PRC1 preserves intestinal stem cell identity by sustaining Wnt/β-catenin transcriptional activity. *Cell Stem Cell* **18**, 91–103 (2016).
52. A. Rossi, K. J. Ferrari, A. Piunti, S. G. Jammula, F. Chiacchiera, L. Mazzarella, A. Scelfo, P. G. Pelicci, D. Pasini, Maintenance of leukemic cell identity by the activity of the Polycomb complex PRC1 in mice. *Sci. Adv.* **2**, e1600972 (2016).
53. V. Kasinath, C. Beck, P. Sauer, S. Poepsel, J. Kosmatka, M. Faini, D. Toso, R. Aebersold, E. Nogales, JARID2 and AEBP2 regulate PRC2 in the presence of H2AK119ub1 and other histone modifications. *Science* **371**, eabc3393 (2021).
54. M. Y. Hamline, C. M. Corcoran, J. A. Wamstad, I. Miletich, J. Feng, J. L. Lohr, M. Hemberger, P. T. Sharpe, M. D. Gearhart, V. J. Bardwell, OFCD syndrome and extraembryonic defects are revealed by conditional mutation of the Polycomb-group repressive complex 1.1 (PRC1.1) gene BCOR. *Dev. Biol.* **468**, 110–132 (2020).
55. S. B. Pierce, M. D. Stewart, S. Gulsuner, T. Walsh, A. Dhall, J. M. McClellan, R. E. Klevit, M.-C. King, De novo mutation in *RING1* with epigenetic effects on neurodevelopment. *Proc. Natl. Acad. Sci. U.S.A.* **115**, 1558–1563 (2018).
56. Y. Wang, P. Chakravarty, M. Ranes, G. Kelly, P. J. Brooks, E. Neilan, A. Stewart, G. Schiavo, J. Q. Svejstrup, Dysregulation of gene expression as a cause of Cockayne syndrome neurological disease. *Proc. Natl. Acad. Sci. U.S.A.* **111**, 14454–14459 (2014).
57. S. Yokotsuka-Ishida, M. Nakamura, Y. Tomiyasu, M. Nagai, Y. Kato, A. Tomiyasu, H. Umehara, T. Hayashi, N. Sasaki, S. I. Ueno, A. Sano, Positional cloning and comprehensive mutation analysis identified a novel KDM2B mutation in a Japanese family with minor malformations, intellectual disability, and schizophrenia. *J. Hum. Genet.* **66**, 597–606 (2021).
58. P. A. Carroll, B. W. Freie, H. Mathsyaraja, R. N. Eisenman, The MYC transcription factor network: Balancing metabolism, proliferation and oncogenesis. *Front. Med.* **12**, 412–425 (2018).
59. P. Llabata, Y. Mitsuishi, P. S. Choi, D. Cai, J. M. Francis, M. Torres-Diz, N. D. Udeshi, L. Golomb, Z. Wu, J. Zhou, T. Svinkina, E. Aguilera-Jimenez, Y. Liu, S. A. Carr, M. Sanchez-Cespedes, M. Meyerson, X. Zhang, Multi-omics analysis identifies MGA as a negative regulator of the MYC pathway in lung adenocarcinoma. *Mol. Cancer Res.* **18**, 574–584 (2020).
60. N. Tanaskovic, M. Dalsass, M. Filipuzzi, G. Ceccotti, A. Verrecchia, P. Nicoli, M. Doni, D. Olivero, D. Pasini, H. Koseki, A. Sabò, A. Bisso, B. Amati, Polycomb group ring finger protein 6 suppresses Myc-induced lymphomagenesis. *Life Sci. Alliance* **14**, e202101344 (2022).
61. A. Astolfi, M. Fiore, F. Melchionda, V. Indio, S. N. Bertuccio, A. Pession, BCOR involvement in cancer. *Epigenomics* **11**, 835–855 (2019).
62. Y. Isshiki, Y. Nakajima-Takagi, M. Oshima, K. Aoyama, M. Rizk, S. Kurosawa, A. Saraya, T. Kondo, E. Sakaida, C. Nakaseko, K. Yokote, H. Koseki, A. Iwama, KDM2B in polycomb repressive complex 1.1 functions as a tumor suppressor in the initiation of T-cell leukemogenesis. *Blood Adv.* **3**, 2537–2549 (2019).
63. T. I. Shaw, L. Dong, L. Tian, C. Qian, Y. Liu, B. Ju, A. High, K. Kavdia, V. R. Pagala, B. Shaner, D. Pei, J. Easton, L. J. Janke, S. N. Porter, X. Ma, C. Cheng, S. M. Pruett-Miller, J. Choi, J. Yu, J. Peng, W. Gu, A. T. Look, J. R. Downing, J. Zhang, Integrative network analysis reveals USP7 haploinsufficiency inhibits E-protein activity in pediatric T-lineage acute lymphoblastic leukemia (T-ALL). *Sci. Rep.* **11**, 5154 (2021).
64. J. A. van der Knaap, E. Kozhevnikova, K. Langenberg, Y. M. Moshkin, C. P. Verrijzer, Biosynthetic enzyme GMP synthetase cooperates with ubiquitin-specific protease 7 in transcriptional regulation of ecdysteroid target genes. *Mol. Cell. Biol.* **30**, 736–744 (2010).
65. A. C. Faesen, A. M. Dirac, A. Shanmugham, H. Ovaa, A. Perrakis, T. K. Sixma, Mechanism of USP7/HAUSP activation by its C-terminal ubiquitin-like domain and allosteric regulation by GMP-synthetase. *Mol. Cell* **44**, 147–159 (2011).
66. M. E. Geijer, D. Zhou, K. Selvam, B. Steurer, C. Mukherjee, B. Evers, S. Cugusi, M. van Toorn, M. van der Woude, R. C. Janssens, Y. P. Kok, W. Gong, A. Raams, C. S. Y. Lo, J. H. G. Lebbink, B. Geverts, D. A. Plummer, K. Bezstarosti, A. F. Theil, R. Mitter, A. B. Houtsmuller, W. Vermeulen, J. A. A. Demmers, S. Li, M. A. T. M. van Vugt, H. Lans, R. Bernards, J. Q. Svejstrup, A. R. Chaudhuri, J. J. Wyrick, J. A. Marteijn, Elongation factor ELOF1 drives transcription-coupled repair and prevents genome instability. *Nat. Cell Biol.* **23**, 608–619 (2021).

Acknowledgments: We thank B. Stielow for generously sharing affinity-purified anti-MGA antibodies. We are grateful to our laboratory members for helpful discussions. We thank M. Timmers and J. Svejstrup for critical reading of the manuscript. **Funding:** This work was supported, in part, by Dutch Research Council ECHO grant no. 711.014.001. **Author contributions:** Conceptualization: A.S. and C.P.V. initiated and designed the study. A.S., J.A.v.d.K., J.W.v.d.M., and G.E.C. conducted most conducted the experiments. K.B., D.H.W.D., W.A.S.D., and J.A.A.D. performed mass spectrometry and proteomics data analysis. Z.O. and W.F.J.v.I. performed next-generation sequencing, and Y.A. performed all the bio-informatic analysis of the RNA-seq and ChIP-Rx-seq experiments. Y.A., A.S., J.A.A.D., and C.P.V. co-wrote the manuscript. All authors discussed results and commented on the manuscript. **Competing interests:** The authors declare that they have no competing interests. **Data and materials availability:** RNA-seq and ChIP-Rx-seq data have been deposited in the Gene Expression Omnibus (GEO) (https://www.ncbi.nlm.nih.gov/geo/) under the accession code GSE193020. The mass spectrometry proteomics data have been deposited to the ProteomeXchange Consortium via the PRIDE partner repository (http://www.proteomexchange.org/) with the dataset identifier PXD030707. All other data needed to evaluate the conclusions in this paper are present in the paper and Supplementary Materials.

Submitted 28 April 2022
Accepted 16 September 2022
Published 4 November 2022
10.1126/sciadv.abq7598

ScienceAdvances

USP7 regulates the ncPRC1 Polycomb axis to stimulate genomic H2AK119ub1 deposition uncoupled from H3K27me3

Ayestha SijmYaser AtlasiJan A. van der KnaapJoyce Wolf van der MeerGillian E. ChalkleyKarel BezstarostiDick H. W. DekkersWouter A. S. DoffZeliha OzgurWilfred F. J. van IJckenJeroen A. A. DemmersC. Peter Verrijzer

Sci. Adv., 8 (44), eabq7598. • DOI: 10.1126/sciadv.abq7598